

NATIONAL ADVISORY COMMITTEE FOR AERONAUTICS

TECHNICAL NOTE 2983

LINEARIZED POTENTIAL THEORY OF PROPELLER
INDUCTION IN A COMPRESSIBLE FLOW

By Robert E. Davidson

Langley Aeronautical Laboratory
Langley Field, Va.



Washington
September 1953

TECHNICAL NOTE 2983

LINEARIZED POTENTIAL THEORY OF PROPELLER

INDUCTION IN A COMPRESSIBLE FLOW

By Robert E. Davidson

SUMMARY

The potential of the linearized flow for a lifting-line propeller of arbitrary circulation distribution at subsonic advance is derived in cylindrical harmonics. From the potential the induced angle at the lifting line is obtained. The series expression for the induced angle is divergent as is to be expected for lifting lines in supersonic flow, but this divergence is removed when the supersonic lifting-line induction is removed. A phenomenon resembling resonance in vibrating systems introduces itself in that one term in the series becomes very large compared to the others. The main consequence of this phenomenon is that the lift distribution cannot be arbitrarily prescribed; on the other hand, the inverse problem, in which the propeller geometry is given, is acceptable.

INTRODUCTION

In order to calculate the induced angle of attack of the propeller blade sections for compressible flow, the velocity potential for the complete flow field must be derived. Inasmuch as the equation of motion changes from an elliptic type to a hyperbolic type at the radius where the propeller blade, or the blade prolonged, is at Mach number one, the disturbance potential turns out to be of mixed elliptic and hyperbolic character. With incompressible flow, the distant boundary condition is certainly that the disturbance potential must be zero far out radially and far upstream. However, with compressible flow, the possibility of propagation of disturbances far ahead, especially in a closed wind tunnel, must be admitted. Therefore, the one problem becomes two; the elliptic field, which is essentially incompressible, and the hyperbolic are determined by different physical conditions.

The velocity potential is obtained by superposing suitable solutions of the compressible equation of motion on the known far-wake velocity

potential, which is also a solution of the compressible equation of motion. This far-wake potential extends only downstream of the propeller and provides the jump in potential at the trailing vortex surfaces and the downstream feature that the far wake must be the same as for incompressible flow except for random wave motion or noise. Therefore, the problem reduces to superposing the elliptic and hyperbolic fields in such a manner that certain physical conditions are met at the propeller plane where the far-wake potential is cut off, an obvious condition being continuity of the velocity vector. The cut-off of the far-wake potential at the propeller plane creates the lifting lines there, since this termination of the surfaces of a potential discontinuity is equivalent to a lifting line.

In the differentiation of the potential at the lifting line, a difficulty is to be anticipated in that a lifting line has infinite wave drag in supersonic flow, and this condition is part of the theory inasmuch as no restrictions are placed on tip Mach number. Some of the hyperbolic induction attributed to the lifting line must therefore be separated. This unwelcome induction is found in the hyperbolic field but is absent in the elliptic field, as would be expected.

For the most part, only the case of propeller operation in a closed circular wind tunnel is considered, although the way the potential may be obtained in free air is indicated. The only reason for emphasizing the tunnel is that, where series occur in the tunnel theory, integrals occur for free air. The series seem more amenable to investigation than the integrals, and it is believed that free air is the limiting case in which the tunnel diameter approaches infinity.

SYMBOLS

B	number of blades
M	advance Mach number, V/a
V	advance velocity
R.P.	real part
a	velocity of sound
$i = \sqrt{-1}$	
t	time
u_a	axial disturbance velocity, positive downstream

u_t	tangential disturbance velocity, positive in direction of propeller rotation
u_z, u_r, u_α	disturbance velocities in positive directions of coordinates z , r , and α , respectively
y'_{nBj}	argument of j th extreme value of Bessel function of order nB
x, ρ, α	dimensionless cylindrical coordinates (eq. (4))
z, r, α	cylindrical coordinates
$\Gamma(\rho)$	circulation at ρ
ϕ	disturbance velocity potential
Φ, Ψ	complementary parts of velocity potential ϕ
α_i	induced angle of attack at blade
$\beta = \sqrt{1 - M^2}$	
ζ	helical angular coordinate (eq. (7))
ρ_a, ρ_T, ρ_S	particular values of ρ for propeller tip, tunnel wall, and sonic radius, respectively
ω	angular velocity, radians per unit time

Subscripts:

i	incompressible
c	compressible

Partial differentiation is indicated by subscripts.

VELOCITY POTENTIAL FOR FLOW IN A CLOSED CIRCULAR WIND TUNNEL

For a linearized theory the disturbance velocity potential ϕ must satisfy the equation

$$\frac{1}{a^2} \phi_{tt} = \phi_{r_2 r_2} + \frac{1}{r_2} \phi_{r_2} + \frac{1}{r_2^2} \phi_{\alpha_2 \alpha_2} + \phi_{z_2 z_2} \quad (1)$$

in which z_2, r_2, α_2 are cylindrical coordinates fixed in the distant fluid, t is the time, and a the velocity of sound. In coordinates which rotate and advance with the propeller, the flow is steady after the propeller has been in operation for a sufficiently long time under constant conditions. Let z_1, r_1, α_1 be the coordinates in the moving system with z_1 along the propeller axis of rotation and with positive directions downstream, outward from the axis, and counter to the propeller rotation, respectively (see fig. 1). If V is the velocity of advance of the propeller and ω the angular velocity, substitution of the transformations

$$z_1 = z_2 + Vt \quad \alpha_1 = \alpha_2 + \omega t \quad r_1 = r_2 \quad (2)$$

into equation (1) leads to the steady-flow equation

$$\phi_{z_1 z_1} \left(1 - \frac{V^2}{a^2}\right) + \phi_{r_1 r_1} + \frac{1}{r_1} \phi_{r_1} + \frac{1}{r_1^2} \phi_{\alpha_1 \alpha_1} \left(1 - \frac{\omega^2 r_1^2}{a^2}\right) - 2\phi_{z_1 \alpha_1} \frac{\omega V}{a^2} = 0 \quad (3)$$

This equation has a more compact form in a third coordinate system x, ρ, α differing from the z_1, r_1, α_1 system only in the length scale; that is,

$$x = \frac{\omega z_1}{V} \quad \rho = \frac{\omega r_1}{V} \quad \alpha = \alpha_1 \quad (4)$$

In this new coordinate system equation (3) becomes

$$\phi_{xx}(1 - M^2) + \phi_{\rho\rho} + \frac{1}{\rho} \phi_{\rho} + \frac{1}{\rho^2} \phi_{\alpha\alpha}(1 - \rho^2 M^2) - 2\phi_{x\alpha} M^2 = 0 \quad (5)$$

In the helical coordinates of Goldstein and Reissner (refs. 1 and 2, respectively) equation (5) becomes

$$\phi_{xx}\beta^2 + \phi_{\rho\rho} + \frac{1}{\rho} \phi_{\rho} + \phi_{\xi\xi}(1 + \rho^{-2}) - 2\phi_{\xi x} = 0 \quad (6)$$

through the transformation

$$\zeta = \alpha - x \quad (7)$$

In the far wake, the oblique system used in equation (6) has advantages because of the helical nature of the flow. However, except for far-wake considerations, equation (5) is preferred because of its orthogonal coordinate system. In equation (6) if $M = 1$, then $\beta = 0$ and the equation suffers the degeneration typical of the linearized equations of flow in that the coefficient of the ϕ_{xx} term is no longer represented by β with sufficient accuracy. Therefore the advance Mach number must not be too close to one.

Equations (5) and (6) may be shown to change from an elliptic type to a hyperbolic type on a cylinder concentric with the propeller axis of rotation with a radius such that the corresponding ρ is

$$\rho_S = \frac{1}{\sqrt{\frac{1}{\beta^2} - 1}} \quad (8)$$

where $\beta = \sqrt{1 - M^2}$. As one would expect, equation (8) defines the cylinder on which the resultant velocity of the undisturbed stream in the moving coordinates is equal to the speed of sound. Because of the change in type of the equation of motion, mixed elliptic and hyperbolic components will generally occur in the complete solution.

The potential given by Reissner in reference 2 for the far wake is already in a usable form for compressible flow because it satisfies equation (5) or (6). This potential is for a propeller of arbitrary circulation distribution. Adapted to the case where a circular wind tunnel is present, Reissner's potential ϕ_w for the far wake takes the form

$$\phi_w = \frac{B\Gamma(\rho)}{2\pi} \zeta + \frac{B}{2\pi} \sum_{n=1}^{\infty} \frac{-2(-1)^n}{nB} h_n(\rho) \sin nB\zeta \quad (9)$$

where

$$h_n(\rho) = -K(\rho) \int_0^\rho I'(\xi) \xi \frac{d\Gamma}{d\xi} d\xi + \frac{I(\rho)K'(\rho_T)}{I'(\rho_T)} \int_0^{\rho_a} I'(\xi) \xi \frac{d\Gamma}{d\xi} d\xi -$$

$$I(\rho) \int_\rho^{\rho_a} K'(\xi) \xi \frac{d\Gamma}{d\xi} d\xi \quad (\rho < \rho_a) \quad (10a)$$

$$h_n(\rho) = \frac{-K(\rho)I'(\rho_T) + I(\rho)K'(\rho_T)}{I'(\rho_T)} \int_0^{\rho_a} I'(\xi) \xi \frac{d\Gamma}{d\xi} d\xi \quad (\rho_a < \rho < \rho_T)$$

(10b)

In these equations ρ_a and ρ_T are the values of ρ for the propeller tip and the tunnel radius, respectively, B is the number of blades, $\Gamma = \Gamma(\rho)$ the circulation distribution depending only on ρ , and $K(\rho)$ and $I(\rho)$ are abbreviations for $K_{nB}(nB\rho)$ and $I_{nB}(nB\rho)$, respectively, which are Bessel functions of imaginary argument. The primes on $K'(\rho)$ and $I'(\rho)$ denote differentiation with respect to ρ , not with respect to the argument $nB\rho$. The angle ζ is zero halfway between vortex sheets from adjacent blades and is limited to $-\frac{\pi}{B} < \zeta < \frac{\pi}{B}$ with the vortex sheets at $\pm \frac{\pi}{B}, \pm \frac{3\pi}{B}, \dots$

It is immediately apparent that the Reissner potential, independent of x , is a solution of equation (6) and hence of equation (5), because for a potential independent of x , equation (5) is Laplace's equation in the ρ, ζ system. Therefore, the Reissner potential equation (9) is considered as the first component of the velocity potential for the propeller with compressible flow, but its region of application is only in back of, or downstream of, the propeller plane. Thus, the jump in ϕ at the helical surfaces trailing from the blades is provided. Therefore, the flow divides naturally into two regions, one in front and the other in back of the propeller plane, both inside the tunnel wall. The rest of the problem consists in adding suitable solutions of equation (5) in front and in back of the propeller in order to take account of the physical conditions.

The appropriate solutions of equation (5) are

$$\mu = J_{nB} \left[\rho \sqrt{\beta^2 \lambda^2 + (nB)^2 \left(\frac{1}{\beta^2} - 1 \right)} \right] e^{inB\alpha} e^{\left[\pm \lambda + inB \left(\frac{1}{\beta^2} - 1 \right) \right] x} \quad (11)$$

as may be verified by direct substitution. The constants n and λ are free. The tunnel-wall boundary condition requires that

$$\rho_T \sqrt{\beta^2 \lambda_{nj}^2 + (nB)^2 \left(\frac{1}{\beta^2} - 1 \right)} = y'_{nBj} \quad (12)$$

where y'_{nBj} is the argument of the Bessel function in equation (11) at the j th extreme value. From equations (8) and (12)

$$\lambda_{nj} = \frac{1}{\beta} \sqrt{\left(\frac{y'_{nBj}}{\rho_T} \right)^2 - \frac{(nB)^2}{\rho_S^2}} \quad (13)$$

where the plus sign is chosen to define λ_{nj} .

Equation (11) now becomes

$$\mu_{\frac{F}{B}} = \left\{ \begin{array}{l} J_{nB} \left(\frac{y'_{nBj}}{\rho_T} \rho \right) \\ J_{nB} \left(\frac{y'_{nBk}}{\rho_T} \rho \right) \end{array} \right\} e^{inB\alpha} \left\{ \begin{array}{l} e^{\left(\pm \lambda_{nj} + i \frac{nB}{\rho_S^2} \right) x} \\ e^{\left[\pm (-i \lambda_{nk}) + \frac{nB}{\rho_S^2} \right] x} \end{array} \right\} \quad (14)$$

The notation $\mu_{\frac{F}{B}}$ refers to μ in front or back of the propeller plane, the F going with the upper sign in the braces, and the B with the lower. The meaning of the two functions, one above the other, in braces is that the upper function is used when λ_{nj} is real, the lower, when

imaginary. It is convenient to use l_{nk} to indicate the imaginary values. The upper function is called, for convenience, the elliptic solution because it dies out exponentially with x , and the lower is called the hyperbolic because it oscillates without dying out. This complication, two possibilities for function character, must be accepted because of the mixed flow.

Two more physical conditions, altogether different, have been imposed in the choice of \pm instead of \mp in equation (14) for the two functions μ in the braces. The origin of x has been set at the propeller plane with x positive downstream; for the elliptic functions the choice of signs is obviously that which makes the solution vanish at $x = \pm\infty$. The choice in the hyperbolic case is such that, since $-il_{nk}$ is positive, the solutions oscillate for given values of n and k with higher frequencies in front than in back of the propeller, in accordance with the physical observation in reference 3 that waves are crossed with higher frequency in front than in back, proceeding in the axial direction.

The rest of the problem is to make superpositions of equation (14) on the Reissner potential, which occupies only the region in back of the propeller, in such a way that the flow is continuous in the propeller plane off the lifting lines.

Because of the discontinuous nature of the first term in equation (9), the compressible fields which must be superposed on the two terms composing equation (9) must be determined separately. For this purpose, let

$$\phi_B = \psi_R + \varphi_R + \psi_B + \psi_{OB} + \varphi_B \quad (0 < x) \quad (15)$$

$$\phi_F = \psi_F + \psi_{OF} + \varphi_F \quad (x < 0) \quad (16)$$

in which ψ_R is the first, or discontinuous, function in Reissner's potential (eq. (9)), φ_R is the second, or continuous one, ψ_F and φ_F are the solutions of the form of equation (14), and ψ_{OB} and ψ_{OF} are degenerate solutions of the form of equation (14) with $n = 0$. Now the origin for the coordinate α must be decided; this is taken to be halfway between

blades. The angles α and ζ are now the same at $x = 0$, with the nearest blades (lifting lines) at $\alpha = \zeta = \pm \frac{\pi}{B}$, $x = 0$. The angles $\zeta = \pm \frac{\pi}{B}$ in the x, ρ, ζ system are at the nearest trailing vortex sheets on each side of $\zeta = 0$.

The compressible potentials ψ_B and ψ_T which accompany the discontinuous Reissner function ψ_R are now determined to provide continuity at the propeller plane. From equation (9)

$$\psi_R = \frac{B\Gamma(\rho)}{2\pi}(\alpha - x) \tag{17a}$$

$$\psi_R = \text{R.P.} \frac{B}{2\pi} \sum_{n=1}^{\infty} \sum_{j=1}^{\infty} \frac{-2(-1)^n}{nB} \Gamma_{nj} J_{nB} \left(\frac{y'_{nBj}}{\rho_T} \rho \right) e^{inB(\alpha-x)} (-i) \tag{17b}$$

where the second form is obtained from an expansion of $\alpha - x$ in a Fourier sine series and another expansion of $\Gamma(\rho)$ in the form

$$\Gamma(\rho) = \sum_{j=1}^{\infty} \Gamma_{nj} J_{nB} \left(\frac{y'_{nBj}}{\rho_T} \rho \right) \tag{18}$$

in which Γ_{nj} is real. This Fourier-Bessel type of expansion is used repeatedly herein. In particular, the arguments of the Bessel functions are always adjusted through the frequency coefficient y'_{nBj}/ρ_T to make the extremes fall at the tunnel wall ρ_T ; in which case Γ_{nj} is given by (see ref. 4, p. 174)

$$\Gamma_{nj} = \frac{2}{\rho_T^2 \left[1 - \left(\frac{nB}{y'_{nBj}} \right)^2 \right] \left[J_{nB}(y'_{nBj}) \right]^2} \int_0^{\rho_T} \rho \Gamma(\rho) J_{nB} \left(\frac{y'_{nBj}}{\rho_T} \rho \right) d\rho \tag{19}$$

The function ψ_R , which is limited to the region downstream of the propeller, causes a discontinuity in the axial velocity and in the potential at the propeller plane $x = 0$. In order to avoid differentiation of equation (17b), the discontinuity in axial velocity brought by ψ_R can be obtained from equation (17a) directly and eliminated with a degenerate term from equation (14) obtained by setting $n = 0$; the result is

$$\psi_{OF} = \frac{B}{2\pi} \sum_{j=1}^{\infty} A_{0j} J_0 \left(\frac{y'_{0j}}{\rho_T} \rho \right) e^{\pm \left(\frac{y'_{0j}}{\beta \rho_T} x \right)} \quad (20)$$

in which A_{0j} is to be determined. No discontinuity of potential is introduced by ψ_{OF} , and the discontinuity in axial velocity is canceled by

$$\left[\frac{\partial}{\partial x} \frac{B\Gamma(\rho)}{2\pi} (\alpha - x) \right]_{x=0} + \left[\frac{\partial \psi_{OB}}{\partial x} \right]_{x=0} = \left[\frac{\partial \psi_{OF}}{\partial x} \right]_{x=0} \quad (21)$$

From equations (17a) and (20), equation (21) becomes

$$-\frac{B\Gamma(\rho)}{2\pi} + \frac{B}{2\pi} \sum_{j=1}^{\infty} -\frac{y'_{0j}}{\beta \rho_T} A_{0j} J_0 \left(\frac{y'_{0j}}{\rho_T} \rho \right) = \frac{B}{2\pi} \sum_{j=1}^{\infty} \frac{y'_{0j}}{\beta \rho_T} A_{0j} J_0 \left(\frac{y'_{0j}}{\rho_T} \rho \right) \quad (22)$$

By using equation (18), the coefficients A_{0j} become

$$A_{0j} = -\frac{1}{2} \frac{\beta \rho_T}{y'_{0j}} \Gamma_{0j} \quad (23)$$

The discontinuity in axial velocity brought by the Reissner term ψ_R is therefore canceled by superposing the potentials

$$\psi_{OF} = \frac{B}{2\pi} \sum_{j=1}^{\infty} - \frac{1}{2} \Gamma_{0j} \frac{\beta \rho_T}{y'_{0j}} J_0 \left(\frac{y'_{0j}}{\rho_T} \rho \right) e^{\pm \frac{y'_{0j}}{\beta \rho_T} x} \quad (24)$$

Only the discontinuity in potential at $x = 0$ caused by ψ_R remains. This discontinuity is canceled by requiring that

$$[\psi_R]_{x=0} + [\psi_B]_{x=0} = [\psi_F]_{x=0} \quad (25)$$

and, in order to prevent introduction of a discontinuity in axial velocity at $x = 0$, by requiring that

$$\left[\frac{\partial}{\partial x} \psi_B \right]_{x=0} = \left[\frac{\partial}{\partial x} \psi_F \right]_{x=0} \quad (26)$$

in which ψ_R comes from equation (17b), and ψ_F is written in the form, adopted from equation (14),

$$\psi_{FB} = \text{R.P.} \frac{B}{2\pi} \sum_{n=1}^{\infty} \sum_{\substack{j=j_0 \\ k=1}}^{j=\infty \\ k=k_0} \frac{-2(-1)^n}{nB} \left\{ \begin{matrix} A_{nj} \psi_{FB} \\ A_{nk} \psi_{FB} \end{matrix} \right\} \left\{ \begin{matrix} J_{nB} \left(\frac{y'_{nBj}}{\rho_T} \rho \right) \\ J_{nB} \left(\frac{y'_{nBk}}{\rho_T} \rho \right) \end{matrix} \right\} e^{inB\alpha} \left\{ \begin{matrix} e^{\left(\pm l_{nj} + i \frac{nB}{\rho_S^2} \right) x} \\ e^{\left(\mp i l_{nk} + \frac{nB}{\rho_S^2} \right) x} \end{matrix} \right\} \quad (27)$$

in which A_{nj} and A_{nk} may be complex; that is,

$$A_{nj} = a_{nj} + ia'_{nj}$$

$$A_{nk} = a_{nk} + ia'_{nk}$$

The range $k = 1, 2, 3, \dots, k_0$ denotes the hyperbolic terms, and $j = j_0, j_{0+1}, j_{0+2}, \dots, \infty$ denotes the elliptic. Here, k_0 denotes the last hyperbolic term in the summation and $j_0 = k_{0+1}$. Substituting equations (17b) and (27) into equation (25) gives

$$\left\{ \begin{array}{l} \Gamma_{nj}(-i) \\ \Gamma_{nk}(-i) \end{array} \right\} + \left\{ \begin{array}{l} a_{njB} + ia'_{njB} \\ a_{nkB} + ia'_{nkB} \end{array} \right\} = \left\{ \begin{array}{l} a_{njF} + ia'_{njF} \\ a_{nkF} + ia'_{nkF} \end{array} \right\} \quad (28)$$

and, similarly, substituting equation (27) into equation (26) gives

$$\left\{ \begin{array}{l} -l_{nj} + i \frac{nB}{\rho_S^2} \\ i \left(il_{nk} + \frac{nB}{\rho_S^2} \right) \end{array} \right\} \left\{ \begin{array}{l} a_{njB} + ia'_{njB} \\ a_{nkB} + ia'_{nkB} \end{array} \right\} = \left\{ \begin{array}{l} l_{nj} + i \frac{nB}{\rho_S^2} \\ i \left(-il_{nk} + \frac{nB}{\rho_S^2} \right) \end{array} \right\} \left\{ \begin{array}{l} a_{njF} + ia'_{njF} \\ a_{nkF} + ia'_{nkF} \end{array} \right\} \quad (29)$$

Equations (28) and (29) each break into two equations corresponding to the real and imaginary parts which yield the following solutions for the elliptic field:

$$\left. \begin{array}{l} a_{njF} = a_{njB} = -\frac{1}{2} \frac{nB}{l_{nj}\rho_S^2} \Gamma_{nj} \\ a'_{njF} = -a'_{njB} = -\frac{1}{2} \Gamma_{nj} \end{array} \right\} \quad (30)$$

and for the hyperbolic field

$$\left. \begin{array}{l} a_{nkF} = a_{nkB} = 0 \\ a'_{nkF} = \frac{1}{2} \Gamma_{nk} \left(-1 + \frac{nB}{-il_{nk}\rho_S^2} \right) \\ a'_{nkB} = \frac{1}{2} \Gamma_{nk} \left(1 + \frac{nB}{-il_{nk}\rho_S^2} \right) \end{array} \right\} \quad (31)$$

The coefficients given by equations (30) and (31) are now to be used in equation (27). Then according to equations (15) and (16), the ψ part of the potential given by collecting equations (17a), (24), and (27) is, for the region in back,

$$\psi_R + \psi_{OB} + \psi_B = \frac{B\Gamma(\rho)}{2\pi}(\alpha - x) + \frac{B}{2\pi} \sum_{j=1}^{\infty} -\frac{1}{2} \Gamma_{0j} \frac{\beta\rho_T}{y'_{0j}} J_0\left(\frac{y'_{0j}}{\rho_T} \rho\right) e^{-\frac{y'_{0j}}{\beta\rho_T} x} +$$

$$\text{R.P.} \frac{B}{2\pi} \sum_{n=1}^{\infty} \sum_{\substack{j=j_0 \\ k=1}}^{\substack{j=\infty \\ k=k_0}} \frac{-2(-1)^n}{nB} \frac{1}{2} \left\{ \begin{array}{l} \Gamma_{nj} \\ \Gamma_{nk} \end{array} \right\} \left\{ \begin{array}{l} \frac{-nB}{l_{nj}\rho_S^2} + i \\ i\left(1 + \frac{nB}{-il_{nk}\rho_S^2}\right) \end{array} \right\} \left\{ \begin{array}{l} J_{nB}\left(\frac{y'_{nBj}}{\rho_T} \rho\right) \\ J_{nB}\left(\frac{y'_{nBk}}{\rho_T} \rho\right) \end{array} \right\} e^{inB\alpha} \left\{ \begin{array}{l} e^{\left(-l_{nj} + i\frac{nB}{\rho_S^2}\right)x} \\ i\left(il_{nk} + \frac{nB}{\rho_S^2}\right)x \end{array} \right\} \quad (32)$$

and in front,

$$\psi_{OF} + \psi_F = \frac{B}{2\pi} \sum_{j=1}^{\infty} -\frac{1}{2} \Gamma_{0j} \frac{\beta\rho_T}{y'_{0j}} J_0\left(\frac{y'_{0j}}{\rho_T} \rho\right) e^{\frac{y'_{0j}}{\beta\rho_T} x} +$$

$$\text{R.P.} \frac{B}{2\pi} \sum_{n=1}^{\infty} \sum_{\substack{j=j_0 \\ k=1}}^{\substack{j=\infty \\ k=k_0}} \frac{-2(-1)^n}{nB} \frac{1}{2} \left\{ \begin{array}{l} \Gamma_{nj} \\ \Gamma_{nk} \end{array} \right\} \left\{ \begin{array}{l} \frac{-nB}{l_{nj}\rho_S^2} - i \\ i\left(-1 + \frac{nB}{-il_{nk}\rho_S^2}\right) \end{array} \right\} \left\{ \begin{array}{l} J_{nB}\left(\frac{y'_{nBj}}{\rho_T} \rho\right) \\ J_{nB}\left(\frac{y'_{nBk}}{\rho_T} \rho\right) \end{array} \right\} e^{inB\alpha} \left\{ \begin{array}{l} e^{\left(l_{nj} + i\frac{nB}{\rho_S^2}\right)x} \\ i\left(-il_{nk} + \frac{nB}{\rho_S^2}\right)x \end{array} \right\} \quad (33)$$

Equations (32) and (33) comprise the final results for the ψ part of the potential ϕ .

Now consider the ϕ part. The procedure is nearly the same, only this time the discontinuity in axial velocity will not be dealt with separately because the ϕ_R part of Reissner's potential is a smooth Fourier development in $\alpha - x$ which can be differentiated. The continuity conditions at the propeller plane $x = 0$ become

$$\left[\phi_R \right]_{x=0} + \left[\phi_B \right]_{x=0} = \left[\phi_F \right]_{x=0} \quad (34)$$

$$\left[\frac{\partial \phi_R}{\partial x} \right]_{x=0} + \left[\frac{\partial \phi_B}{\partial x} \right]_{x=0} = \left[\frac{\partial \phi_F}{\partial x} \right]_{x=0} \quad (35)$$

in which ϕ_R is the second term in equation (9). This term may be written, in the x, ρ, α system, as

$$\phi_R = \text{R.P.} \frac{B}{2\pi} \sum_{n=1}^{\infty} \frac{-2(-1)^n}{nB} h_n(\rho) e^{inB(\alpha-x)} (-i) \quad (36)$$

or, alternatively,

$$\phi_R = \text{R.P.} \frac{B}{2\pi} \sum_{n=1}^{\infty} \sum_{j=1}^{\infty} \frac{-2(-1)^n}{nB} h_{nj} J_{nB} \left(\frac{y'_{nBj}}{\rho_T} \rho \right) e^{inB(\alpha-x)} (-i) \quad (37)$$

where

$$h_n(\rho) = \sum_{j=1}^{\infty} h_{nj} J_{nB} \left(\frac{y'_{nBj}}{\rho_T} \rho \right) \quad (38)$$

and h_{nj} is real.

The $\Phi_{\frac{F}{B}}$ are obtained from equation (27) with ψ replaced by ϕ and some new coefficients B_{nj} substituted for A_{nj} .

The ϕ part of the potential now becomes, with the B_{nj} determined from equations (34) and (35) in a manner similar to that for A_{nj} ,

$$\Phi_R + \Phi_B = \text{R.P.} \frac{B}{2\pi} \sum_{n=1}^{\infty} \frac{-2(-1)^n}{nB} h_n(\rho) e^{inB(\alpha-x)} (-i) +$$

$$\text{R.P.} \frac{B}{2\pi} \sum_{n=1}^{\infty} \sum_{\substack{j=j_0 \\ k=1}}^{\substack{j=\infty \\ k=k_0}} \frac{-2(-1)^n}{nB} \frac{1}{2} \left\{ \begin{array}{l} h_{nj} \\ h_{nk} \end{array} \right\} \left\{ \begin{array}{l} \frac{-nB}{l_{nj}\beta^2} + i \\ i \left(1 + \frac{nB}{-il_{nj}\beta^2} \right) \end{array} \right\} \left\{ \begin{array}{l} J_{nB} \left(\frac{y'_{nBj}}{\rho_T} \rho \right) \\ J_{nB} \left(\frac{y'_{nBk}}{\rho_T} \rho \right) \end{array} \right\} e^{inB\alpha} \left\{ \begin{array}{l} e^{\left(-l_{nj} + i \frac{nB}{\rho_S^2} \right) x} \\ i \left(il_{nk} + \frac{nB}{\rho_S^2} \right) x \\ e \end{array} \right\}$$

(39)

$$\Phi_F = \text{R.P.} \frac{B}{2\pi} \sum_{n=1}^{\infty} \sum_{\substack{j=j_0 \\ k=1}}^{\substack{j=\infty \\ k=k_0}} \frac{-2(-1)^n}{nB} \frac{1}{2} \left\{ \begin{array}{l} h_{nj} \\ h_{nk} \end{array} \right\} \left\{ \begin{array}{l} \frac{-nB}{l_{nj}\beta^2} - i \\ i \left(-1 + \frac{nB}{-il_{nk}\beta^2} \right) \end{array} \right\} \left\{ \begin{array}{l} J_{nB} \left(\frac{y'_{nBj}}{\rho_T} \rho \right) \\ J_{nB} \left(\frac{y'_{nBk}}{\rho_T} \rho \right) \end{array} \right\} e^{inB\alpha} \left\{ \begin{array}{l} e^{\left(l_{nj} + i \frac{nB}{\rho_S^2} \right) x} \\ i \left(-il_{nk} + \frac{nB}{\rho_S^2} \right) x \\ e \end{array} \right\}$$

(40)

Equations (39) and (40) added to equations (32) and (33) determine the velocity potential for the propeller in accordance with equations (15) and (16).

PRANDTL INDUCED VELOCITIES AT THE LIFTING LINE

The Prandtl induced velocities, in the sense used herein, are analogous to those of the conventional lifting-line wing and propeller theories of Prandtl and Goldstein. More specifically, the Prandtl induced velocities are those which must be presumed to be already present at the position of the blades in order to assume that the airfoils retain locally their same performance as in two-dimensional flow. With incompressible flow, it was verified experimentally that the induction could be determined with sufficient accuracy by assuming the wing or blade to shrink into a lifting line and then applying the Biot-Savart law over the trailing vortices excluding the lifting line. This simplification of the intrinsic general three-dimensional problem has long since proved its worth. Therefore it is natural to seek extensions in approaching the compressible problem. On the other hand, it is dangerous to rely on experience with incompressible flow for guidance in supersonic matters. Since the present problem concerns a mixed subsonic and supersonic flow, it will be expected that questions will arise which will have to be settled by considerations of both subsonic and supersonic flow. Finally, for those who are more interested in the general three-dimensional problem rather than an engineering concept, it is remarked that the theory is still applicable to a lifting-surface problem when those steps are omitted which specialize to the lifting line.

The induced velocities, or disturbance velocities, are given by differentiations of ϕ , but the algebraic sign is still open to a choice which is made so that a forward-thrusting propeller pushes the air rearward in the far wake. If the propeller is assumed to produce positive thrust when $\Gamma(\rho)$ is positive, then the velocities in the positive directions of the coordinates must be

$$u_{z_1} = -\phi_{z_1} \quad u_{r_1} = -\phi_{r_1} \quad u_{\alpha_1} = -\frac{1}{r_1} \phi_{\alpha_1} \quad (41)$$

which may be checked by means of the Reissner ψ_R term, which produces the basic disturbance velocity in the far wake, as follows:

Since

$$\psi_R = \frac{B\Gamma(\rho)}{2\pi} \left(\alpha_1 - \frac{\omega}{V} z_1 \right)$$

u_{α_1} is seen to be negative, but since the propeller rotates in the negative α_1 direction, u_{α_1} is a velocity in the same direction as the rotation, as it should be; on the other hand, u_{z_1} is positive, but since z_1 is positive downstream, u_{z_1} is positive downstream, also as it should be.

In propeller theory, it is customary to consider an axial velocity u_a and a tangential velocity u_t , which are positive downstream and in the direction of propeller rotation. Since u_{z_1} is positive downstream, but u_{α_1} is positive against the propeller rotation, $u_a = u_{z_1}$ and $u_t = -u_{\alpha_1}$. Therefore, from equations (41) and (4)

$$u_a = -\frac{\omega}{V} \phi_x \tag{42}$$

$$u_t = \frac{\omega}{V} \frac{1}{\rho} \phi_\alpha \tag{43}$$

determine the conventional axial and tangential velocities from the velocity potential in the x, ρ, α system.

It is immaterial whether the differentiations in equations (42) and (43) are applied to ϕ_F or ϕ_B when the differentiation, which is not straightforward, is made at the lifting lines. Suppose ϕ_B is used and consider first the ψ part of ϕ (eq. (32)). For the ψ_x differentiation, the second term in equation (32) cancels one-half of the first term. If it is permissible to differentiate the remaining term, then at $x = 0$ and $\alpha = \frac{\pi}{B}$, which means the lifting line,

$$\left[\frac{\partial}{\partial x} (\psi_R + \psi_{OB} + \psi_B) \right]_{\substack{x=0 \\ \alpha=\frac{\pi}{B}}} = \frac{1}{2} \frac{\partial \psi_R}{\partial x} + \frac{B}{2\pi} \sum_{n=1}^{\infty} \sum_{k=1}^{k_0} \frac{-2(-1)^n}{nB} \frac{1}{2} \Gamma_{nk} J_{nB} \left(\frac{y'_{nBk}}{\rho_T} \rho \right) (-1)^n \left[-i l_{nk} - \frac{(nB)^2}{-i l_{nk} \rho_S^4} \right] \tag{44}$$

that is, the ψ part of ϕ_x at the lifting line is one-half of the far-wake value plus some effects from the hyperbolic part of the compressible field. The differentiation in the α direction is made with regard for the Fourier development of the saw-tooth function which can be recognized in equation (32) at $x = 0$. For $x = 0$ it is seen that the i in the first brace gives a term

$$\text{R.P. } \frac{B}{2\pi} \sum_{n=1}^{\infty} \sum_{\substack{k=k_0 \\ j=j_0 \\ k=1}}^{j=\infty} \frac{-2(-1)^n}{nB} \frac{1}{2} \left\{ \begin{array}{l} \Gamma_{nj} \\ \Gamma_{nk} \end{array} \right\} \left\{ \begin{array}{l} J_{nB} \left(\frac{y'_{nBj}}{\rho_T} \rho \right) \\ J_{nB} \left(\frac{y'_{nBk}}{\rho_T} \rho \right) \end{array} \right\} (i) e^{inB\alpha}$$

but from equation (17b) this term is just

$$- \frac{1}{2} \frac{B\Gamma(\rho)}{2\pi} \alpha$$

and, therefore, the differentiation of this term cancels one-half of the differentiation of the first term in equation (32). In other words, the derivative of the above Fourier series with respect to α is to be interpreted as the derivative of the sloping part of a saw-tooth function of α which the series actually represents, the differentiation being performed off the teeth of the saw-tooth function. This choice of interpretation is justified by the fact that by so doing the theory gives the correct results when degenerated to incompressible flow.

Since $\text{R.P.}(e^{inB\alpha})$ contributes nothing at $\alpha = \frac{\pi}{B}$, formal differentiation of the rest of equation (32) gives

$$\left[\frac{\partial}{\partial \alpha} (\psi_R + \psi_{OB} + \psi_B) \right]_{x=0} = \frac{1}{2} \frac{\partial \psi_R}{\partial \alpha} +$$

$$\frac{B}{2\pi} \sum_{n=1}^{\infty} \sum_{k=1}^{k_0} \frac{-2(-1)^n}{nB} \frac{1}{2} \Gamma_{nk} J_{nB} \left(\frac{y'_{nBk}}{\rho_T} \rho \right) \frac{(-1)^n}{-1} \frac{(nB)^2}{-i l_{nk} \rho_S^2}$$

(45)

Therefore, the ψ part of ϕ_α is also one-half of the far-wake value plus some effects from the hyperbolic field.

Next equation (39) is differentiated. The differentiation of the real part along x , for $x = 0$ and $\alpha = \frac{\pi}{B}$, gives

$$\frac{\partial}{\partial x}(\varphi_R + \varphi_B) = \frac{B}{2\pi} \sum_{n=1}^{\infty} \frac{-2(-1)^n}{nB} h_n(\rho) \frac{(-1)^n}{-1} nB +$$

$$\frac{B}{2\pi} \sum_{n=1}^{\infty} \sum_{\substack{j=j_0 \\ k=1}}^{\substack{j=\infty \\ k=k_0}} \frac{-2(-1)^n}{nB} \frac{1}{2} \begin{Bmatrix} h_{nj} \\ h_{nk} \end{Bmatrix} \begin{Bmatrix} J_{nB} \left(\frac{y'_{nBj}}{\rho_T} \rho \right) \\ J_{nB} \left(\frac{y'_{nBk}}{\rho_T} \rho \right) \end{Bmatrix} (-1)^n \left\{ \begin{array}{c} nB \\ nB + \left[-il_{nk} - \frac{(nB)^2}{-il_{nk}\beta^2\rho_S^2} \right] \end{array} \right\}$$

(46)

However, from equation (38), the nB terms in the last brace cancel one-half of the φ_R term by the same considerations as for equation (45). Therefore, equation (46) becomes

$$\left[\frac{\partial}{\partial x}(\varphi_R + \varphi_B) \right]_{\substack{x=0 \\ \alpha=\frac{\pi}{B}}} = \frac{1}{2} \frac{\partial \varphi_R}{\partial x} + \frac{B}{2\pi} \sum_{n=1}^{\infty} \sum_{k=1}^{k_0} \frac{-2(-1)^n}{nB} \frac{1}{2} h_{nk} J_{nB} \frac{y'_{nBk}}{\rho_T} \rho (-1)^n \left[-il_{nk} - \frac{(nB)^2}{-il_{nk}\beta^2\rho_S^2} \right]$$

(47)

and, similarly,

$$\left[\frac{\partial}{\partial \alpha} (\phi_R + \phi_B) \right]_{x=0, \alpha=\frac{\pi}{B}} = \frac{1}{2} \frac{\partial \phi_R}{\partial \alpha} + \frac{B}{2\pi} \sum_{n=1}^{\infty} \sum_{k=1}^{k_0} \frac{-2(-1)^n}{nB} \frac{1}{2} h_{nk} J_{nB} \left(\frac{y'_{nBk}}{\rho_T} \rho \right) \frac{(-1)^n}{-1} \frac{(nB)^2}{i l_{nk} \beta^2} \quad (48)$$

Equations (44), (45), (47), and (48) give ϕ_x and ϕ_α at the lifting line, but they must be expected to include some induction from the lifting line itself. This part of the induction must be discarded in order to have the Prandtl induced velocities at the lifting line. It should be possible to recognize the induction of the lifting line from an inspection of equations (44), (45), (47), and (48). In equations (44) and (45), the double summation has coefficients Γ_{nk} which depend directly on the circulation distribution $\Gamma(\rho)$ along the lifting line; whereas h_{nk} in equations (47) and (48) depend on $h_n(\rho)$ which expresses the field produced by $\Gamma(\rho)$. Therefore, the hyperbolic terms in equations (44) and (45) are now discarded as being caused by the lifting line itself.

Some further explanation of this step is perhaps desirable. It is this operation which makes the lifting-line concept applicable although the flow has partly supersonic character. The lifting line in supersonic flow has infinite wave drag which shows up in the fact that the velocities associated with the ψ part of the Reissner potential are expressed by series which do not converge (eqs. (44) and (45)). Furthermore, if the theory is allowed to degenerate to the case of a large number of blades at a large distance from the axis so that the potential may be considered independent of radius, the representation of an infinite staggered cascade in supersonic flow is obtained, the properties of which are already known. Then the hyperbolic terms in equations (44) and (45) are seen to represent just the self-induced field of each cascade element by itself. On the other hand, it is the self-induced field which must be taken out in order to obtain the Prandtl induced velocities. Therefore the indicated rejection is in accordance with the lifting-line concept.

Substitution of equations (44) and (47) into equation (42) gives

$$\bar{u}_{a_c} = \bar{u}_{a_i} - \frac{B}{2\pi} \frac{\omega}{V} \sum_{n=1}^{\infty} \sum_{k=1}^{k_0} \frac{-2(-1)^n}{nB} \frac{1}{2} h_{nk} J_{nB} \left(\frac{y'_{nBk}}{\rho_T} \rho \right) (-1)^n \left[-i l_{nk} - \frac{(nB)^2}{-i l_{nk} \beta^2 \rho_S^2} \right] \quad (49)$$

and substitution of equations (45) and (48) into equation (43) gives

$$\bar{u}_{t_c} = \bar{u}_{t_i} + \frac{B}{2\pi} \frac{1}{\rho} \frac{\omega}{V} \sum_{n=1}^{\infty} \sum_{k=1}^{k_0} \frac{-2(-1)^n}{nB} \frac{1}{2} h_{nk} J_{nB} \left(\frac{y'_{nBk}}{\rho_T} \rho \right) \frac{(-1)^n}{-1} \frac{(nB)^2}{-i l_{nk} \beta^2} \quad (50)$$

in which the bars denote the Prandtl induced velocity, the subscripts *c* and *i* refer to compressible and incompressible, respectively, and the terms in Γ_{nk} have been discarded.

DISCUSSION

The Bessel functions in equations (49) and (50) are those shown in figure 2. It is shown subsequently that these functions are distributed over the radius in such a way that the first inflection point of the Bessel function in the k_0 th term falls on or very near the sonic radius. For the lower *k* terms the first inflection point is progressively more outboard of the sonic cylinder so that at $k = 1$ it is near the tunnel wall with the first extreme (a maximum) of the Bessel function right at the tunnel wall. For $k = 2$, the second extreme (a minimum) is at the tunnel wall, and so forth for the succeeding values of *k* as is seen from inspection of the arguments of the Bessel functions (see fig. 3). Finally, at $k = k_0$, which is the hyperbolic term with the largest *k*, the maximum number of oscillations of the Bessel function occur and these oscillations are all confined between the sonic cylinder and the tunnel wall, because as was pointed out above, the first inflection point of the k_0 th Bessel function falls at or near the sonic cylinder.

The process of distributing the Bessel functions over the radius influences the values of l_{nk} obtained from equation (13). This fact brings up the significant point that l_{nk_0} can approach zero and thus produce an effect similar to resonance in a vibrating system; each narrow range of conditions for resonance is an extra degree reduced by

the square-root operation in equation (13). An identically zero value of l_{nk_0} means that some additional considerations are required. However, when later the case of a propeller in free air is taken up, the summations over j and k pass to radial integrations in which the difficulty of zero l_{nk_0} appears as a square-root singularity which causes no trouble and provides the first hint that a near-zero value for l_{nk} is to be regarded as a necessary feature of the theory due to a resonance property of the flow in a tunnel.

Generation of the coefficients h_{nk} .- The coefficients h_{nk} are those in a Fourier-Bessel expansion of the Reissner far-wake radial function $h_n(\rho)$. The functions $h_n(\rho)$ have the appearance shown in figure 3. The function $h_n(\rho)$ has a discontinuity in its first derivative because, when $h_n(\rho)$ is added to Γ , the resulting function must be smooth in order to make equation (9) give a continuous flow at $\rho = \rho_a$. Also sketched in figure 3 are the Bessel functions for given values of nB used in the expansion of $h_n(\rho)$. These functions have their extreme values on the tunnel wall ρ_T as is required by the arguments $\frac{y_{nBk}}{\rho_T} \rho$. Only the Bessel functions for the hyperbolic terms in the velocity potential are shown, the ones appearing in equations (49) and (50). The value $k = 1$ corresponds to the Bessel function with the first extreme value at $\rho = \rho_T$ because, from the argument $\frac{y_{nBk}}{\rho_T} \rho$, when ρ ranges from $\rho = 0$ to ρ_T it generates the Bessel function up to the first extreme value. The k_0 th function is the one with first inflection point and ρ_S nearly coinciding. Thus, for the case represented, k takes on the values $k = 1$ to $k = k_0 = 4$ which correspond to hyperbolic terms in the velocity potential. The terms with higher numbers of extremes are not shown because they have elliptic flow character, and they would merely produce more and more oscillatory portions inboard of the sonic cylinder $\rho = \rho_S$.

It has been stated that the first inflection point of the k_0 th Bessel function falls at or near the sonic radius. A more precise statement, however, would be that the k_0 th Bessel function has its argument equal to its order at or near the sonic radius. However, the inflection point has more meaning for visualization purposes. Furthermore, it can be shown that the argument at the first inflection point is nearly equal to the order, if the order is not too small, with considerable error as may be seen from figure 2. This coincidence that the k_0 th Bessel function tends to have an argument equal to the order at or near the sonic radius will now be demonstrated and it is to be inferred that this coincidence also applies to the first inflection point. It will appear that the coincidence of the argument with the

order is exact if $l_{nk_0} = 0$. For a zero value of l_{nk_0} , equation (12) shows that

$$\rho_T \frac{nB}{\rho_S} = y'_{nBk_0}$$

or,

$$\frac{y'_{nBk_0}}{\rho_T} \rho_S = nB \quad (51)$$

which states that the argument of the k_0 th Bessel function is equal to the order nB at the sonic cylinder $\rho = \rho_S$ if l_{nk_0} is exactly zero.

If l_{nk_0} is not exactly zero, then equation (51) is still nearly true. Thus, from equation (12)

$$\frac{y'_{nBk}}{\rho_T} \rho_S = \sqrt{(nB)^2 + \rho_S^2 \beta^2 l_{nk}^2} \quad (52)$$

which shows that since l_{nk} is imaginary, corresponding to hyperbolic terms, the argument of the Bessel function at the sonic cylinder is less than nB . The reverse would be true if the terms were elliptic so that l_{nk} would be real from equation (12). It appears then that, in figure 3, the k_0 th Bessel function has its argument equal to nB just outboard of or at ρ_S , depending on whether l_{nk_0} is merely close to zero or identically zero. Further, the hyperbolic terms with k lower than k_0 have their oscillatory portions more and more outboard of the sonic cylinder $\rho = \rho_S$ as k decreases from k_0 .

The sonic cylinder and tunnel-wall radius in relation to the first appearance of hyperbolic solutions in the velocity potential.- The hyperbolic solutions first enter the velocity potential when the sonic cylinder comes inside the tunnel wall. If equation (13) is written in the form

$$l_{nk} = \frac{1}{\beta} \frac{nB}{\rho_T} \sqrt{\left(\frac{y'_{nBk}}{nB}\right)^2 - \left(\frac{\rho_T}{\rho_S}\right)^2}$$

then since the hyperbolic solutions have imaginary l_{nk} the proof of this statement is seen to consist in showing that the smallest possible value for $\frac{y'_{nBk}}{nB}$ is unity, which is shown to occur when $k_0 = 1$ and $nB \rightarrow \infty$. This proof will place a lower limit on ρ_T for the occurrence of imaginary l_{nk} ; that is, ρ_T must be greater than ρ_S for imaginary l_{nk} to occur. Therefore, the solutions cannot change type unless the tunnel wall is outside the sonic cylinder. It is obvious that the smallest value of $\frac{y'_{nBk}}{nB}$ must occur for $k = 1$ because with this value of k the argument of the first extreme must be less than all succeeding arguments. It, therefore, remains to show that the smallest value for $\frac{y'_{nB1}}{nB}$ is unity, which follows from a formula on page 143 of reference 5 that holds when nB is large,

$$\frac{y'_{nB1}}{nB} \approx 1 + \frac{0.808618 \sqrt[3]{nB}}{nB} + \dots \quad (53)$$

Hence

$$\lim_{nB \rightarrow \infty} \frac{y'_{nB1}}{nB} = 1 \quad (54)$$

which completes the proof.

Diagrammatic point of view of zero l_{nk_0} in relation to the argument of the Bessel function.- Figure 4 gives a view looking down the vertical axis in figure 2 showing the traces of the extremes of $J_{nB}(y)$ on the nB, y plane. The slopes of these traces approach unity as nB and y become large, a property of the Bessel function. For a given propeller operating condition, ρ_T and ρ_S may be calculated; by plotting in figure 4 the function $\frac{\rho_T}{\rho_S} nB$, it is possible to tell by inspection of the figure how many hyperbolic solutions are present in each k -wise summation, and the possibility of a zero value for l_{nk_0} may be appreciated. From equation (51), the condition for zero l_{nk_0} is

$$y'_{nBk_0} = \frac{\rho_T}{\rho_S} nB \tag{55}$$

If the line $\frac{\rho_T}{\rho_S} nB$ intersects one of the traces of the extremes on an integral value of nB , then the corresponding l_{nk_0} will be zero. For example, if the dashed line through the origin in figure 4 represents $\frac{\rho_T}{\rho_S} nB$ for a given operating condition, then l_{nk_0} for $nB = 8$ and $k = k_0 = 2$ would be zero.

The dashed line in figure 4 may also be taken as an indication of what parts of the Bessel functions $J_{nB}(y)$ are used for the elliptic and what parts for the hyperbolic solutions at any given operating condition. Equation (13) shows this separation because imaginary l_{nk} are given by equation (13) so that the solutions are hyperbolic when

$$\frac{(nB)^2}{\rho_S^2} > \left(\frac{y'_{nBk}}{\rho_T} \right)^2$$

or

$$nB \frac{\rho_T}{\rho_S} > y'_{nBk}$$

which means that for hyperbolic solutions, the traces of the extremes y'_{nBk} must be below the dashed line $\frac{\rho_T}{\rho_S} nB$. Since the slopes of traces of the extremes approach unity as $nB \rightarrow \infty$, the first appearance of hyperbolic solutions occurs when $\frac{\rho_T}{\rho_S} = 1$, because for this case the line $\frac{\rho_T}{\rho_S} nB$ also has slope unity (shown as the solid straight line through the origin in fig. 4).

The suppression of resonant terms.- The discussion of the resonant terms is based on the assumption that in the series expression for the induced velocities, or the induced angle of attack at the blade, only one zero of l_{nk_0} can occur within a finite number of terms in the

series. In the author's opinion, this is true but a rigorous proof is lacking. From a practical point of view, the series does not need to be computed to a great number of terms, because the higher terms express their contributions to the induced angle through oscillatory functions of higher and higher frequency so that they eventually become unimportant in a practical solution. Thus the question of how many resonant terms must be dealt with can be answered for practical purposes by the fact that in a series of a reasonable number of terms only one zero of l_{nk_0} can occur at a time so that there is just one resonant term.

Consider a propeller operating at conditions which make a particular l_{nk_0} exactly zero. With this zero of l_{nk_0} is associated a resonant term or mode in the series expression for the induced angle of attack. Now suppose the propeller to be twisted so that the angle of attack with respect to the zero-lift angles of the airfoil sections is equal to the resonant mode multiplied by some finite constant factor. This propeller, according to the theory, is subject to degenerate compressibility effects, which can be seen without calculation as follows:

(1) Since infinite induced velocities are physically impossible, it is seen from equations (49) and (50) that h_{nk_0} must be zero; that is, the lift distribution of the propeller must be such that h_{nk_0} is zero so that the ratio $\frac{h_{nk_0}}{l_{nk_0}} = \frac{0}{0}$ appearing in those equations has a finite value.

(2) The only value for h_{nk_0}/l_{nk_0} which produces zero h_{nk_0} is that which makes the resonant induced angle exactly cancel the blade twist so that the lift is zero all along the blade.

Therefore the only solution compatible to both the compressible and incompressible components of the induction is that the lift remains zero with the indeterminate ratio h_{nk_0}/l_{nk_0} taking whatever value is necessary to make the resonant mode exactly compensate the prescribed angle of attack. It seems reasonable to expect a similar suppression of the resonant mode when the angle-of-attack distribution is arbitrary. Therefore, in compressible flow, the arbitrary prescription of lift must always be made with the restriction that h_{nk_0} for the resonant mode be zero. The corresponding propeller geometry is seen to be indeterminate in that the geometric angle of attack can be altered in proportion to the induced angle of the resonant mode without changing the prescribed lift distribution.

The other problem, in which the propeller geometry is given instead of the lift distribution, is more realistic. Here, the lift distribution must again yield no resonant mode ($h_{nk_0} = 0$) and is determined

according to the requirement that the lifting properties of the blade and the induced angles due to all the modes including the resonant mode with finite h_{nk_0}/l_{nk_0} must produce the lift distribution by which the modes are determined. In practice this solution would be obtained by an iteration process.

Assume a propeller of fixed geometry. The lift distribution, or otherwise $\Gamma(\rho)$, is to be determined along the blade. If the resonant term is assumed to be zero, such a distribution along with the distribution of induced velocities and induced angles can be determined. Suppose, however, that a resonant term occurs in the induced velocities and, correspondingly, in the induced angles. The induced angles are then infinitely sensitive to small changes in the lift distribution and some special considerations are necessary.

The lift distribution with the resonant term assumed to be zero will in general produce some value of the resonant coefficient $(h_{nk_0})_r$. To prevent the introduction of infinite induced angles and thus to make the lift distribution consistent with the induced-angle distribution, the lift distribution must be so modified as to result in zero values of h_{nk_0} so that h_{nk_0}/l_{nk_0} will be finite.

Suppose that $\frac{h_{nk_0}}{l_{nk_0}} = 1$, and compute the corresponding change of induced angle $\Delta\alpha_1(\rho)$ and the accompanying change in circulation distribution $\Delta\Gamma(\rho)$. From $\Delta\Gamma(\rho)$ compute Δh_{nk_0} from equations 10(a) and 10(b), and an equation similar to (19). Now because $h_n(\rho) \propto \Gamma(\rho)$ and $\Delta\Gamma(\rho) \propto \Delta\alpha_1(\rho)$, take C so that

$$C \Delta h_{nk_0} = -(h_{nk_0})_r \quad (56)$$

and adjust the induced angles and the circulation by adding $C \Delta\alpha_1(\rho)$ and $C \Delta\Gamma(\rho)$, respectively. This is equivalent to taking $\frac{h_{nk_0}}{l_{nk_0}} = C$ where $h_{nk_0} = l_{nk_0} = 0$. The process is inexact, of course, because of the effect of the added $\Delta\Gamma(\rho)$ on the induced velocities, and successive approximations are therefore required.

The above iteration process may be performed mentally on the hypothetical propeller defined at the beginning of this section in which the propeller was twisted with an angle of attack with respect

to the zero-lift angle of the airfoil sections equal to the induced angle of attack of the resonant mode multiplied by a constant factor. It will be seen that the process gives the correct result, which is zero lift over the whole blade. The validity of the iteration process is thus confirmed to the extent that the abovementioned hypothetical propeller actually does produce no lift. The latter question appears to require experimental verification. This requirement is not surprising when it is recalled that the Prandtl lifting-line wing theory, in which lifting lines were to be replaceable by finite chords of the same circulation, could not be rigorously justified and had to await experimental verification.

VELOCITY POTENTIAL IN FREE AIR

The velocity potential in free air has a form different from that where a tunnel is present; the difference is analogous to the change of a Fourier series into an integral when the interval of expansion becomes infinitely great. As far as the induced velocities are concerned, it is believed that they will be not much different from those with the tunnel present. Therefore, the free-air potential will not be derived in detail.

From Hankel's integral (see eq. (3) on p. 453 of ref. 6)

$$F_n(R) = \int_0^\infty \gamma \, d\gamma \int_0^\infty F_n(s) J_{nB}(\gamma s) J_{nB}(\gamma R) s \, ds \quad (57)$$

the function Φ_R in the Reissner potential as $\rho_T \rightarrow \infty$ can be represented by

$$\Phi_R = \text{R.P.} \frac{B}{2\pi} \sum_{n=1}^{\infty} \frac{-2(-1)^n}{nB} \int_0^\infty \gamma f_n(\gamma) J_{nB}(\gamma \rho) e^{inB(\alpha-x)} (-1) d\gamma \quad (58)$$

where $F_n(R)$ becomes $h_n(\rho)$ by comparison with equation (36) and the function $f_n(\gamma)$ is given by

$$f_n(\gamma) = \int_0^\infty h_n(x) J_{nB}(\gamma s) ds \quad (59)$$

The function $h_n(\rho)$ used here must suit the boundary conditions of the far wake, obtained from equations (10) by letting $\rho_T \rightarrow \infty$.

By analogy with equation (11) and by using a form of equation (57), choose

$$\Phi_{\frac{F}{B}} = \frac{B}{2\pi} \sum_{n=1}^{\infty} \frac{-2(-1)^n}{nB} \int_0^{\infty} C_{n\frac{F}{B}}(\gamma) \gamma f_n(\gamma) J_{nB}(\gamma\rho) e^{inB\alpha} e^{\left[\frac{1}{\beta} \sqrt{\gamma^2 - \frac{(nB)^2}{\rho_S^2} + i \frac{nB}{\rho_S^2}} \right] x} d\gamma \tag{60}$$

which is a solution of equation (5) if differentiation under the integral is permissible. The physical conditions may now be imposed by methods similar to those in the case where a tunnel was present. It will be found

that the functions $C_n(\gamma)$ contain the radical $\sqrt{\gamma^2 - \frac{(nB)^2}{\rho_S^2}}$ in the denominator, and this radical is the counterpart of l_{nj} (see eq. (13)). Therefore, the summation over j for the tunnel case passes to an integration over γ where the possible infinity caused by l_{nj} in the denominator becomes in free air a square-root singularity in the integration, which should cause no difficulty.

NUMERICAL EXAMPLE

A two-blade propeller is assumed to operate at an advance Mach number M of 0.8193, with ρ at the tip equal to unity; therefore, the advance ratio V/nD is π , and the circulation distribution is

$$\Gamma^*(\rho) = \frac{1}{6} \rho \sqrt{1 - \rho^2} \tag{61}$$

where

$$\Gamma^* = \frac{B\omega}{V^2} \Gamma \tag{62}$$

is a nondimensional form for Γ and V/nD is the conventional parameter in which nD is the angular velocity in revolutions per unit time multiplied by propeller diameter D . The circulation Γ^* is plotted in figure 5, from equation (61), along with the corresponding induced quantities \bar{u}_{a_i}/V , \bar{u}_{t_i}/V , and α_{i_1} , where α_{i_1} is the induced angle of attack for incompressible flow expressed in radians. No particular significance is to be attached to the factor $1/6$ in equation (61) or to the precise choice $M = 0.8193$.

If equations (49) and (50) are written as

$$\bar{u}_{a_c} = \bar{u}_{a_i} + \Delta u_a \quad (63)$$

$$\bar{u}_{t_c} = \bar{u}_{t_i} + \Delta u_t \quad (64)$$

where Δu_a and Δu_t are the changes due to compressibility, then

$$\Delta u_a = -\frac{B}{2\pi} \frac{\omega}{V} \sum_{n=1}^{\infty} \sum_{k=1}^{k_0} \frac{-2(-1)^n}{nB} \frac{1}{2} h_{nk} J_{nB} \left(\frac{y'_{nBk}}{\rho_T} \rho \right) (-1)^n \left[-i\lambda_{nk} - \frac{(nB)^2}{-i\lambda_{nk}\beta^2\rho_S^2} \right] \quad (65)$$

$$\Delta u_t = \frac{B}{2\pi} \frac{1}{\rho} \frac{\omega}{V} \sum_{n=1}^{\infty} \sum_{k=1}^{k_0} \frac{-2(-1)^n}{nB} \frac{1}{2} h_{nk} J_{nB} \left(\frac{y'_{nBk}}{\rho_T} \rho \right) \frac{(-1)^n}{-1} \frac{(nB)^2}{-i\lambda_{nk}\beta^2} \quad (66)$$

If h_{nk}^* , based on Γ^* instead of Γ , is defined as

$$h_{nk}^* = \frac{B\omega}{V^2} h_{nk} \quad (67)$$

the compressibility effects in ratio to the incompressible can be determined from equations (65) and (66) as follows:

$$a_c = \frac{\Delta u_a/V}{\bar{u}_{a_i}/V} = \frac{1}{4\pi} \frac{1}{\bar{u}_{a_i}/V} \sum_{n=1}^{\infty} \sum_{k=1}^{k_0} a_{nk}(\rho) \quad (68)$$

$$t_c = \frac{\Delta u_t/V}{\bar{u}_{t_i}/V} = \frac{1}{4\pi\rho} \frac{1}{\bar{u}_{t_i}/V} \sum_{n=1}^{\infty} \sum_{k=1}^{k_0} t_{nk}(\rho) \quad (69)$$

where

$$a_{nk}(\rho) = \frac{2}{nB} h_{nk}^* J_{nB} \left(\frac{y'_{nBk}}{\rho_T} \rho \right) \left[-i l_{nk} - \frac{(nB)^2}{-i l_{nk} \beta^2 \rho_S^2} \right] \quad (70)$$

$$t_{nk}(\rho) = \frac{2}{nB} h_{nk}^* J_{nB} \left(\frac{y'_{nBk}}{\rho_T} \rho \right) \frac{(nB)^2}{-i l_{nk} \beta^2} \quad (71)$$

The coefficients h_{nk}^* and $-i l_{nk}$ are tabulated in tables I and II for the first six terms in the n -wise summation. These coefficients, with the very complete tabulation of the Bessel functions in reference 7, are used to calculate $a_{nk}(\rho)$ and $t_{nk}(\rho)$ which are tabulated in tables III and IV.

The ratios $\frac{\Delta u_a/V}{\bar{u}_{a_i}/V}$ and $\frac{\Delta u_t/V}{\bar{u}_{t_i}/V}$ which express the compressibility effects in ratio to the velocities in incompressible flow are plotted against ρ in figure 6. The compressibility effect is seen to be very small, less than 4 percent.

Before discussing the induced angle of attack, some explanation of the velocity diagrams in figure 7 may be desirable. Figure 7(a) shows the conventional velocity diagram of incompressible-flow propeller theory. Figure 7(b) shows the compressibility effects superposed on the incompressible. Since only the part of the diagram showing the induced velocities is important, an enlargement of this part is shown in figure 7(c). The lines A-A, B-B, and C-C which are the sides of the induced angles may all be drawn parallel to the local helical direction in a small-disturbance flow.

If $\Delta\alpha_i$ is the change in induced angle of attack accompanying Δu_a and Δu_t , then from figure 7

$$\Delta\alpha_i = \frac{\frac{\rho \Delta u_a}{\sqrt{1 + \rho^2}} + \frac{\Delta u_t}{\sqrt{1 + \rho^2}}}{V \sqrt{1 + \rho^2}} = \frac{1}{1 + \rho^2} \left[\rho a_c \frac{\bar{u}_{a_i}}{V} + t_c \frac{\bar{u}_{t_i}}{V} \right] \quad (72)$$

which, by using equations (68) and (69), can be put in the form

$$\frac{\Delta\alpha_i}{\alpha_{i_i}} = \frac{1}{4\pi} \frac{1}{\alpha_{i_i}} \sum_{n=1}^{\infty} \sum_{k=1}^{k_0} \alpha_{nk}(\rho) \quad (73)$$

where

$$\alpha_{nk}(\rho) = \frac{1}{1 + \rho^2} \left[\rho a_{nk}(\rho) + \frac{1}{\rho} t_{nk}(\rho) \right] \quad (74)$$

Values of $\alpha_{nk}(\rho)$ are tabulated in table V. The ratio $\Delta\alpha_i/\alpha_{i_i}$ plotted in figure 6 is seen to be very small; this fact indicates that the induced efficiency is reduced only 1 or 2 percent by compressibility, to the accuracy provided by six terms in the summation over n .

In figure 8, partial sums of $\alpha_{nk}(\rho)$ are plotted so that the contribution of succeeding terms can be seen. There is a shift in the convergence with the addition of the fifth term. This shift is caused by an unusually large h_{nk}^* at $n = 5$, $k_0 = 3$.

It should be noted that, although the induced angle has been calculated for a prescribed circulation distribution, nothing is said about the shape of the propeller required to give this circulation distribution. At some n , there may be an Γ_{nk} sufficiently close to zero so that a strongly oscillatory induced-angle distribution is finally indicated and an unusual blade-angle distribution would result. Apparently, a degree of arbitrariness is lost in giving arbitrary circulation distributions if they are to be related to reasonably shaped propellers. More realistic is the view that the propeller shape is prescribed and then the performance is calculated. This approach would mean in the present example that, after the calculation of the induced angle, its effect on the initial circulation distribution would be calculated, after which the new distribution would be used for a new induced-angle calculation. In the process, the resonant mode would be suppressed, and a reasonable induced-angle distribution and a circulation distribution somewhat different from that of the prescribed propeller in an incompressible flow would result.

CONCLUDING REMARKS

The velocity potential for a lifting-line propeller with subsonic advance velocity but unrestricted tip speed has been derived in cylindrical harmonics. The theory is for a linear equation of motion and must be restricted to advance Mach numbers not too close to one.

From the velocity potential, the induction at the blade has been obtained with a view to preserving a strict analogy to the induced-angle-of-attack concept embodied in Prandtl's lifting-line wing theory which has been carried over to propellers by Goldstein and Reissner.

The Prandtl induced angle of attack becomes representable by the basic incompressible results plus some compressibility effects expressed in infinite series. Among the terms in the series there is always at least one which becomes magnified with indefinite greatness in comparison with the others, an effect resembling resonance in vibration theory.

A numerical example is provided in which a limited number of terms in the series expression for the induced angle of attack have been calculated for a propeller with a reasonable lift distribution. The compressibility effect appears to be negligibly small, but it must be noted that there was no resonant term among the terms calculated. It is remarked that the arbitrary prescription of the lift distribution cannot be made if resonance is to be considered.

Although the present calculation indicates that the nonresonant terms in the velocity potential produce only a small compressibility

effect on the induction at the blade, it is not certain that the resonant term, or near-resonant terms, would not make a significant contribution. In other words, if an example were chosen for calculation in which the propeller geometry were prescribed instead of the lift distribution, and if the operating conditions of the propeller were chosen to make a certain convenient term resonant, then, after completing a somewhat laborious iteration process, a significant compressibility effect might be observed as a result of the direct consideration of the relation of resonance to a realistic physical problem. It is the author's opinion that the calculation could probably be made with sufficient accuracy by considering only the induction of the Reissner potential and the resonant term with the nonresonant terms neglected. One might be led further to expect such a calculation to explain the experimentally observed dips in the lift distributions of propellers operating at tip speeds above a Mach number of 1.00; unfortunately, the explanation would not be completely clear, however, because there is always the uncertain effect of compressibility on the airfoil properties in the transonic range which is probably a considerable cause of the dips in the lift distribution.

With regard to experimental verifications there is one check which would seem to be satisfactorily definite. It consists in testing a propeller in a circular wind tunnel at an operating condition producing an exact resonance for a particular term or mode in the series expression for the induced angle of attack. If the blade-angle distribution for the blade is so designed that the airfoils have, with respect to zero lift, an angle-of-attack distribution the same as (or differing only by a constant factor from) the induced angle of attack of the resonant mode, then, according to the theory, the propeller could support no load. The propeller would need to be constructed with some accuracy in the blade-angle distribution but the other design particulars would be arbitrary. In particular, the airfoils might just as well be symmetric.

Langley Aeronautical Laboratory,
National Advisory Committee for Aeronautics,
Langley Field, Va., July 7, 1953.

REFERENCES

1. Goldstein, Sydney: On the Vortex Theory of Screw Propellers. Proc. Roy. Soc. (London), ser. A, vol. 123, no. 792, Apr. 6, 1929, pp. 440-465.
2. Reissner, H.: On the Relation Between Thrust and Torque Distribution and the Dimensions and the Arrangement of Propeller-Blades. Phil. Mag., ser. 7, vol. 24, no. 163, Nov. 1937, pp. 745-771.
3. Busemann, Adolf: Theory of the Propeller in Compressible Flow. Presented at Third Midwestern Conference on Fluid Mechanics (Minneapolis, Minn.), Mar. 22-24, 1953.
4. Smythe, William R.: Static and Dynamic Electricity. McGraw-Hill Book Co., Inc., 1939.
5. Jahnke, Eugene, and Emde, Fritz: Tables of Functions With Formulae and Curves. Rev. ed., Dover Publications (New York), 1943.
6. Watson, G. N.: A Treatise on the Theory of Bessel Functions. Second ed., The Macmillan Co., 1944.
7. Staff of the Computation Laboratory: The Annals of the Computation Laboratory of Harvard University. Tables of the Bessel Functions of the First Kind of Orders Zero to One Hundred Thirty-Five. Vols. III-XIV, Harvard Univ. Press, 1947-51.

TABLE I.- COEFFICIENTS h_{nk}^*

$k \backslash n$	1	2	3	4	5	6
1	0.010442	0.008512	0.005774	0.003776	0.002412	0.001485
2			-.000300	.003183	.003381	.003089
3					-.005847	-.000830


 NACA
TABLE II.- TABULATION OF $-il_{nk}$

$k \backslash n$	1	2	3	4	5	6
1	3.4966	7.8164	12.1428	16.4777	20.8245	25.1683
2			6.1113	11.4201	15.9732	20.4635
3					8.2499	14.1980


 NACA

TABLE III.- ESSENTIAL PART OF THE INDUCED-AXIAL-VELOCITY CALCULATION $a_{nk}(\rho)$

$n \backslash k$	1	2	3	4	5	6
$\rho = 0.3$						
1	-0.001702	-0.000066	-0.000003	-----	-----	-----
2			.000009	-0.000006	-----	-----
3					0.000017	-----
$\sum_{k=1}^{k_0}$	-.001702	-.000066	.000006	-.000006	.000017	-----
$\rho = 0.4$						
1	-0.002949	-0.000198	-0.000014	-0.000001	-----	-----
2			.000043	-.000049	-0.000007	-0.000001
3					.000222	.000004
$\sum_{k=1}^{k_0}$	-.002949	-.000198	.000029	-.000050	.000215	.000003
$\rho = 0.5$						
1	-0.004468	-0.000457	-0.000051	-0.000006	-0.000001	-----
2			.000134	-.000229	-.000051	-0.000010
3					.001384	.000037
$\sum_{k=1}^{k_0}$	-.004468	-.000457	.000083	-.000235	.001332	.000027
$\rho = 0.6$						
1	-0.006192	-0.000881	-0.000138	-0.000023	-0.000004	-0.000001
2			.000308	-.000735	-.000226	-.000062
3					.005122	.000194
$\sum_{k=1}^{k_0}$	-.006192	-.000881	.000170	-.000758	.004892	.000131
$\rho = 0.7$						
1	-0.008036	-0.001499	-0.000307	-0.000066	-0.000014	-0.000003
2			.000560	-.001756	-.000711	-.000257
3					.012522	.000630
$\sum_{k=1}^{k_0}$	-.008036	-.001499	.000253	-.001822	.011797	.000370
$\rho = 0.8$						
1	-0.009944	-0.002311	-0.000593	-0.000160	-0.000044	-0.000012
2			.000838	-.003296	-.001670	-.000756
3					.020977	.001352
$\sum_{k=1}^{k_0}$	-.009944	-.002311	.000245	-.003456	.019263	.000584
$\rho = 0.9$						
1	-0.011811	-0.003298	-0.001017	-0.000330	-0.000109	-0.000036
2			.001040	-.004963	-.003040	-.001662
3					.023273	.001907
$\sum_{k=1}^{k_0}$	-.011811	-.003298	.000023	-.005293	.020124	.000209

TABLE IV.- ESSENTIAL PART OF THE INDUCED-TANGENTIAL-VELOCITY CALCULATION $t_{nk}(\rho)$

$n \backslash k$	1	2	3	4	5	6
$\rho = 0.3$						
1	0.001643	0.000084	0.000004	-----	-----	-----
2			-0.000005	0.000004	-----	-----
3					-0.000009	-----
$\sum_{k=1}^{k_0}$.001643	.000084	-0.000001	.000004	-0.000009	-----
$\rho = 0.4$						
1	0.002846	0.000252	0.000021	0.000002	-----	-----
2			-0.000026	.000035	0.000006	0.000001
3					-0.000122	-0.000002
$\sum_{k=1}^{k_0}$.002846	.000252	-0.000005	.000037	-0.000116	-0.000001
$\rho = 0.5$						
1	0.004312	0.000581	0.000074	0.000009	0.000001	-----
2			-0.000079	.000167	.000042	0.000009
3					-0.000761	-0.000024
$\sum_{k=1}^{k_0}$.004312	.000581	-0.000005	.000176	-0.000718	-0.000015
$\rho = 0.6$						
1	0.005976	0.001121	0.000198	0.000035	0.000006	0.000001
2			-0.000181	.000535	.000188	.000057
3					-0.002818	-0.000123
$\sum_{k=1}^{k_0}$.005976	.001121	.000017	.000570	-0.002624	-0.000065
$\rho = 0.7$						
1	0.007756	0.001909	0.000442	0.000102	0.000023	0.000005
2			-0.000330	.001280	.000591	.000237
3					-0.006889	-0.000398
$\sum_{k=1}^{k_0}$.007756	.001909	.000112	.001382	-0.006275	-0.000156
$\rho = 0.8$						
1	0.009598	0.002942	0.000853	0.000247	0.000071	0.000020
2			-0.000493	.002403	.001389	.000697
3					-0.011541	-0.000855
$\sum_{k=1}^{k_0}$.009598	.002942	.000360	.002650	-0.010081	-0.00138
$\rho = 0.9$						
1	0.011400	0.004198	0.001464	0.000511	0.000177	0.000060
2			-0.000612	.003618	.002529	.001532
3					-0.012804	-0.001206
$\sum_{k=1}^{k_0}$.011400	.004198	.000852	.004129	-0.010098	.000386

TABLE V.- ESSENTIAL PART OF THE INDUCED-ANGLE-OF-ATTACK CALCULATION $\alpha_{nk}(\rho)$

k \ n	1	2	3	4	5	6
$\rho = 0.3$						
1 2 3	0.004557	0.000239	0.000012 -0.000012	----- 0.000009	----- -0.000021	----- -----
$\sum_{k=1}^k$.004557	.000239	0	.000009	-.000021	-----
$\sum_{n=1}^n \sum_{k=1}^k$.004557	.004796	.004796	.004805	.004784	0.004784
$\rho = 0.4$						
1 2 3	0.005116	0.000474	0.000041 -0.000041	0.000004 .000058	----- .000011 -0.000185	----- 0.000002 -0.000002
$\sum_{k=1}^k$.005116	.000474	0	.000062	-.000174	0
$\sum_{n=1}^n \sum_{k=1}^k$.005116	.005590	.005590	.005652	.005478	.005478
$\rho = 0.5$						
1 2 3	0.005112	0.000747	0.000038 -0.000072	0.000011 .000176	0.000002 .000046 -0.000664	----- 0.000010 -0.000024
$\sum_{k=1}^k$.005112	.000747	.000026	.000187	-.000615	-.000014
$\sum_{n=1}^n \sum_{k=1}^k$.005112	.005859	.005885	.006072	.005456	.005442
$\rho = 0.6$						
1 2 3	0.004592	0.000985	0.000181 -0.000086	0.000033 .000331	0.000006 .000131 -0.01194	0.000001 .000043 -0.000065
$\sum_{k=1}^k$.004592	.000985	.000035	.000364	-.001057	-.000021
$\sum_{n=1}^n \sum_{k=1}^k$.004592	.005577	.005672	.006036	.004979	.004958
$\rho = 0.7$						
1 2 3	0.003661	0.001126	0.000280 -0.000054	0.000067 .000403	0.000015 .000233 -0.000722	0.000004 .000106 -0.000085
$\sum_{k=1}^k$.003661	.001126	.000226	.000470	-.000474	.000025
$\sum_{n=1}^n \sum_{k=1}^k$.003661	.004787	.005013	.005483	.005009	.005034
$\rho = 0.8$						
1 2 3	0.002465	0.001115	0.000361 .000033	0.000111 .000224	0.000033 .000244 .001436	0.000014 .000162 .000008
$\sum_{k=1}^k$.002465	.001115	.000394	.000335	.001713	.000184
$\sum_{n=1}^n \sum_{k=1}^k$.002465	.003580	.003974	.004309	.005022	.006206
$\rho = 0.9$						
1 2 3	0.001125	0.000937	0.000393 .000141	0.000150 -0.000247	0.000055 .000041 .003712	0.000019 .000114 .000208
$\sum_{k=1}^k$.001125	.000937	.000534	-.000097	.003808	.000341
$\sum_{n=1}^n \sum_{k=1}^k$.001125	.002062	.002596	.002499	.006307	.006648



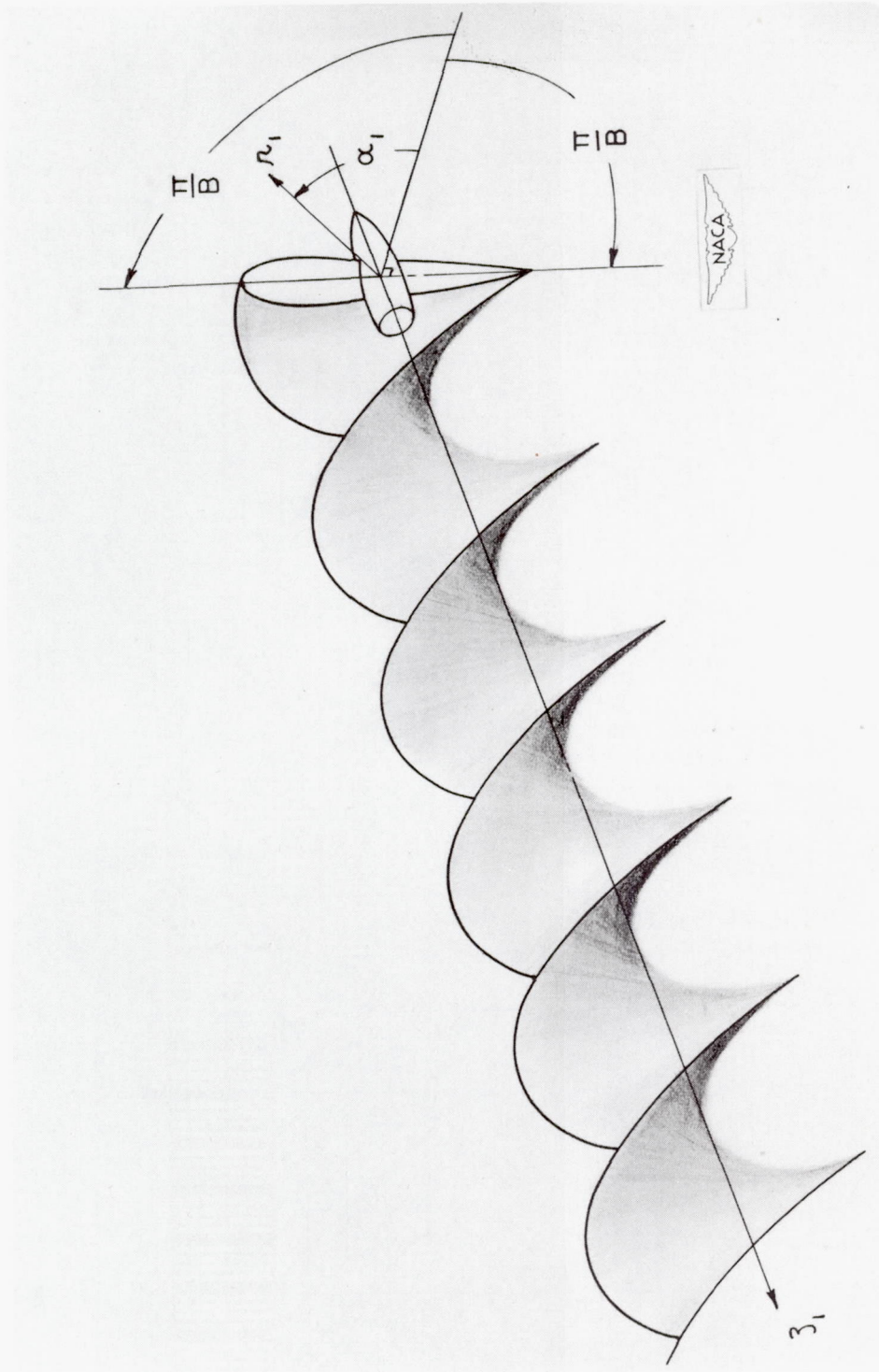


Figure 1.- Orientation of cylindrical coordinate system.

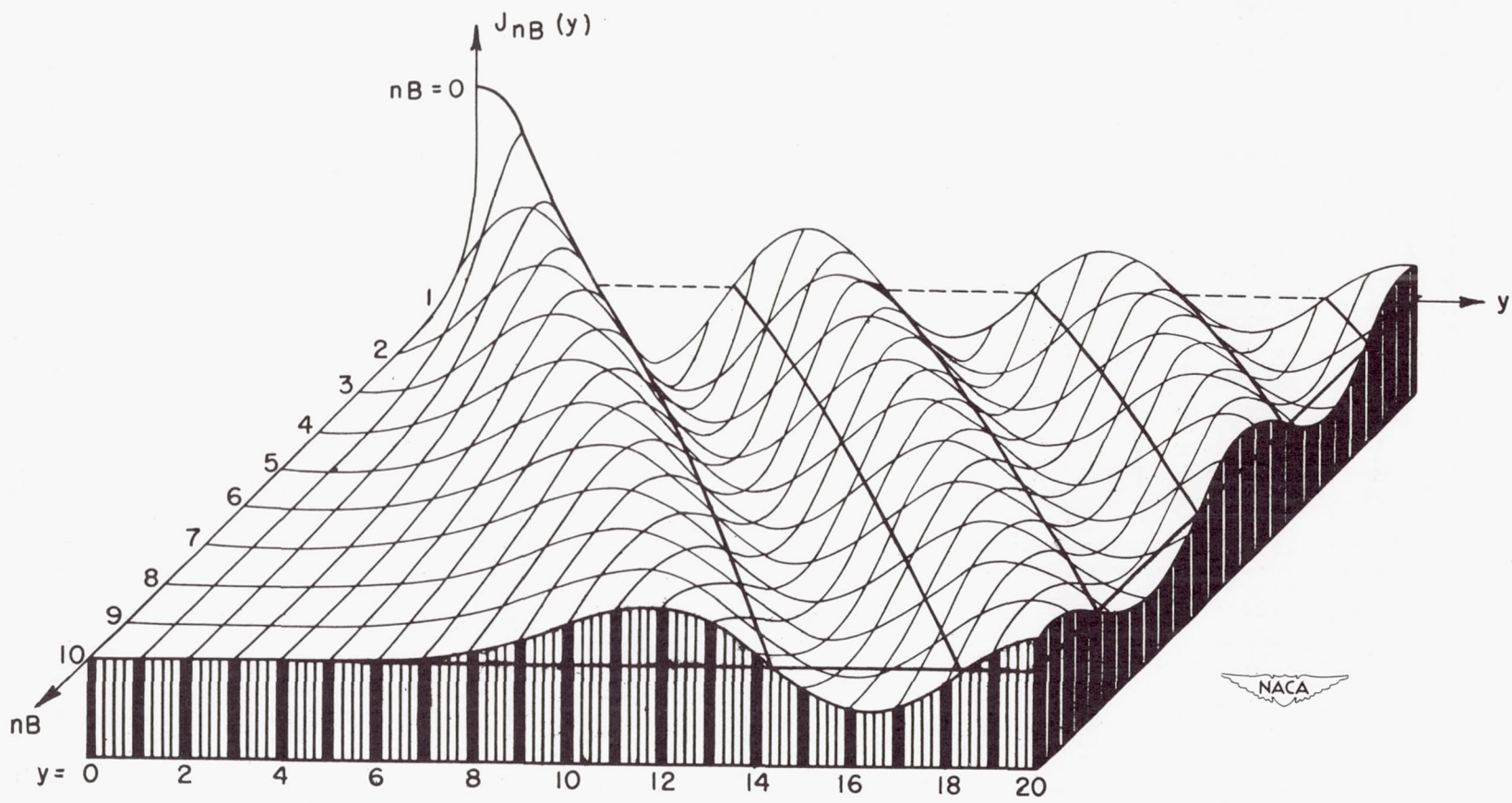


Figure 2.- The function $J_{nB}(y)$.

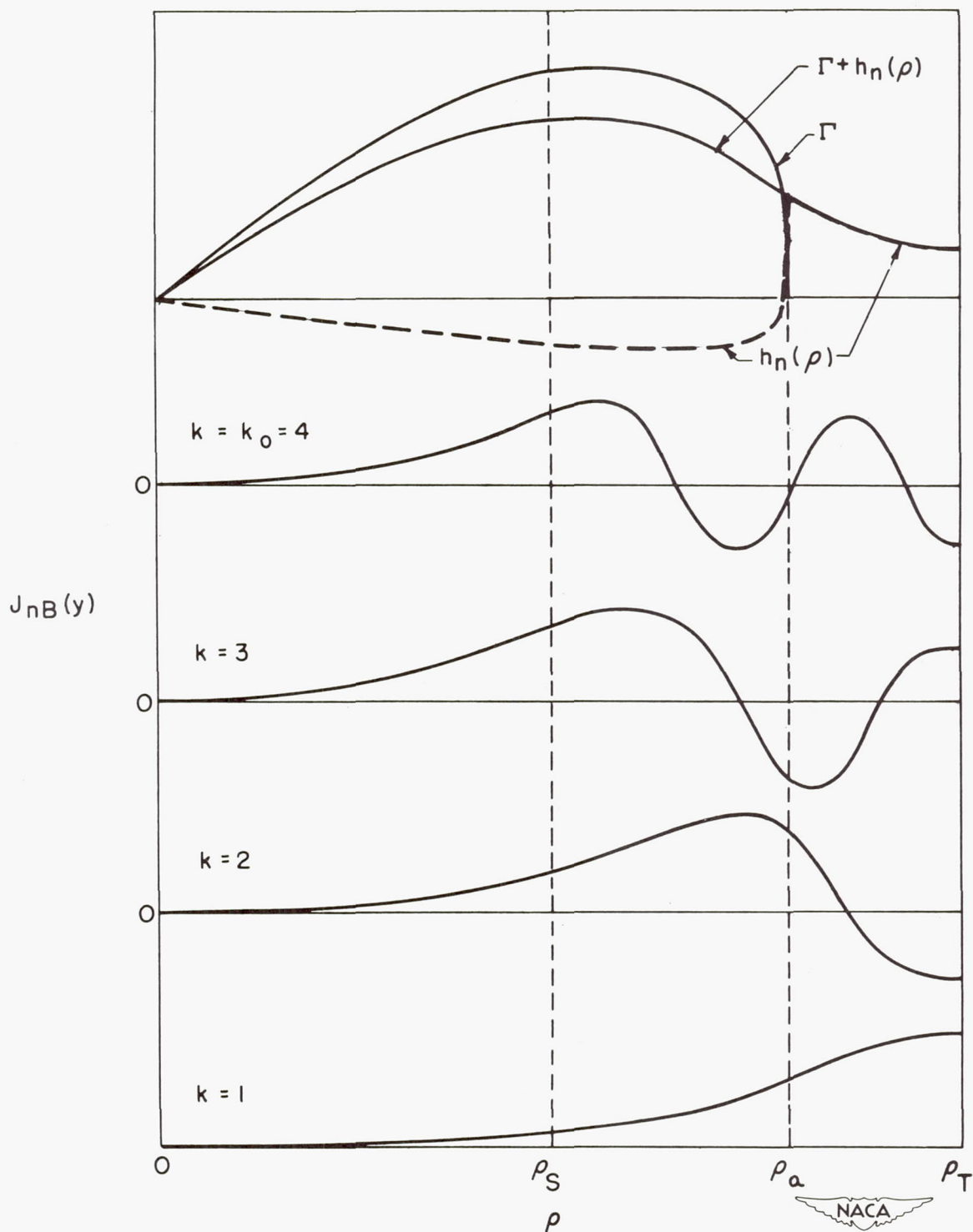


Figure 3.- Schematic representation of the Bessel functions $J_{nB}(y)$ in relation to the functions $\Gamma(\rho)$ and $h_n(\rho)$.

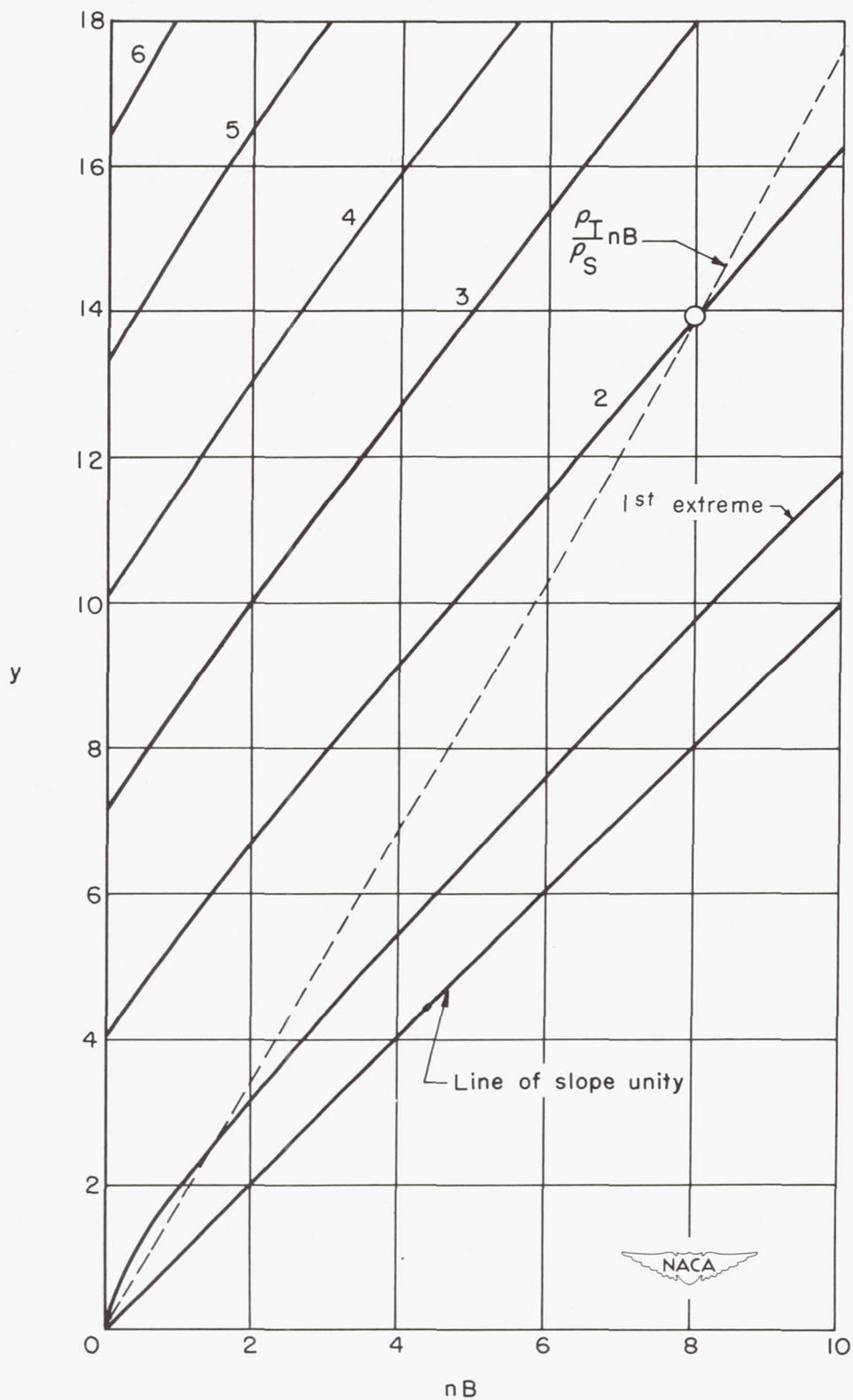


Figure 4.- Traces of the extremes of $J_{nB}(y)$ on the nB, y plane.

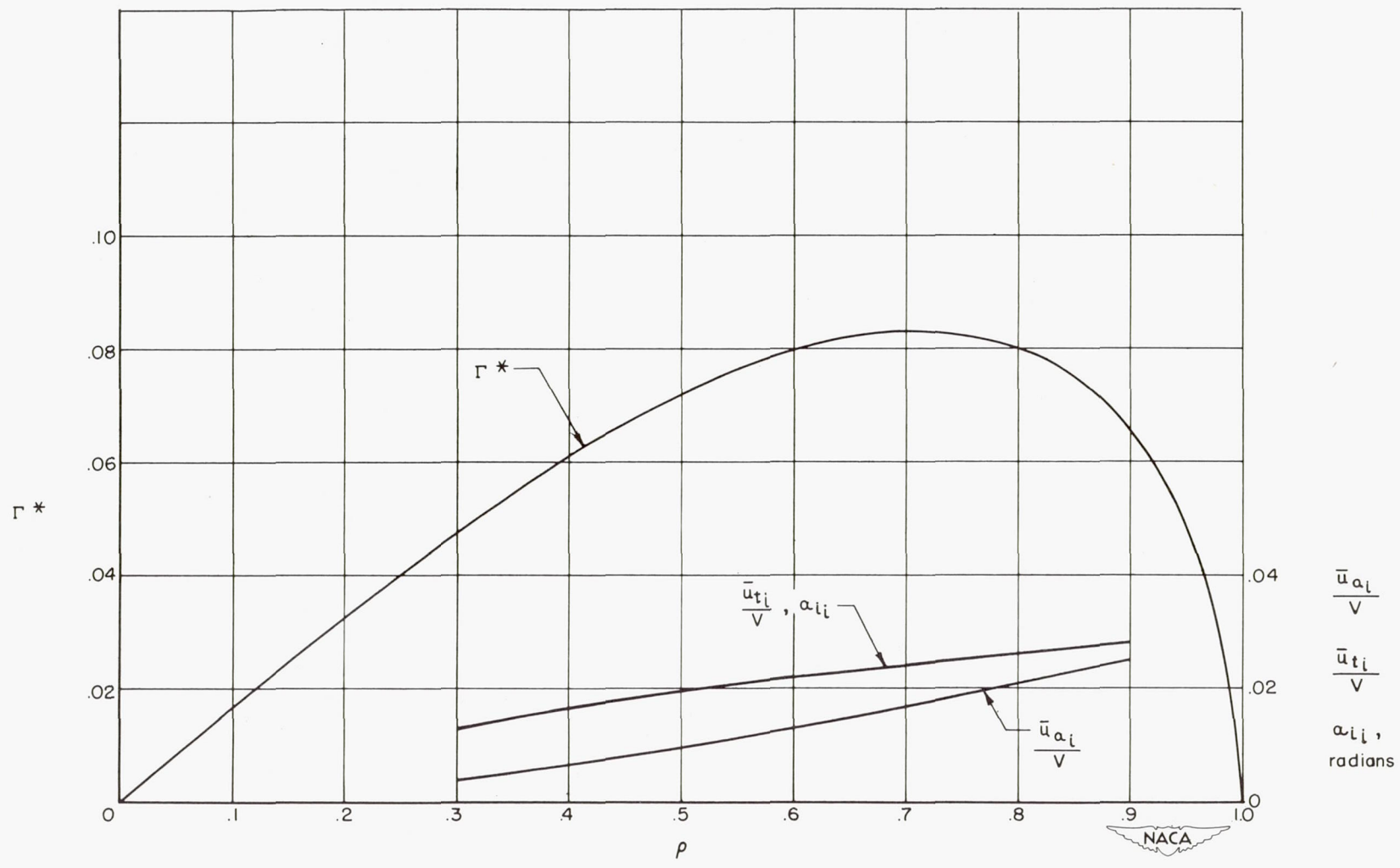


Figure 5.- Circulation distribution and corresponding incompressible induced quantities. $\Gamma^* = \frac{1}{6} \rho \sqrt{1 - \rho^2}$; $B = 2$.

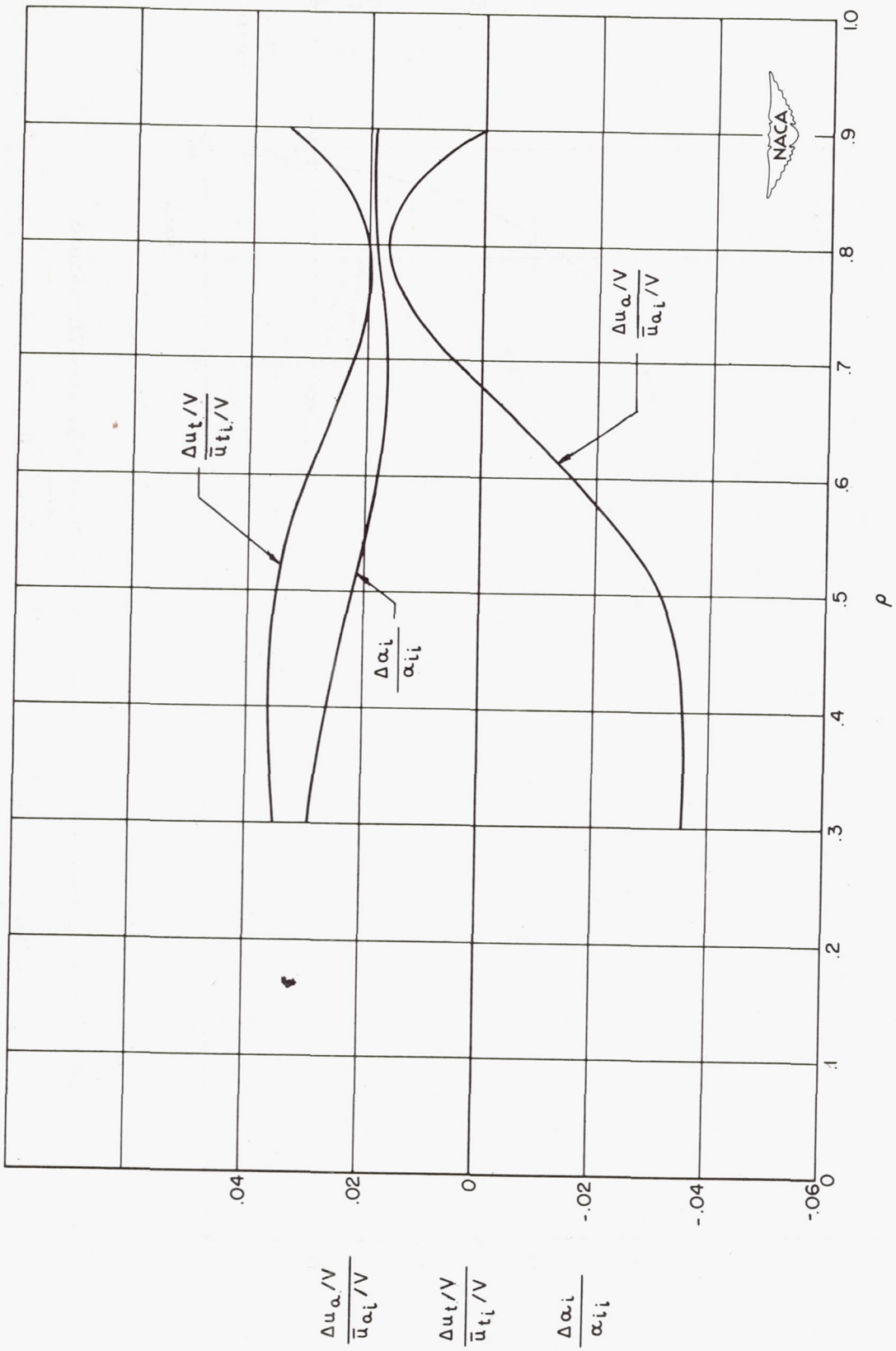


Figure 6.- Compressible induction at the blade.

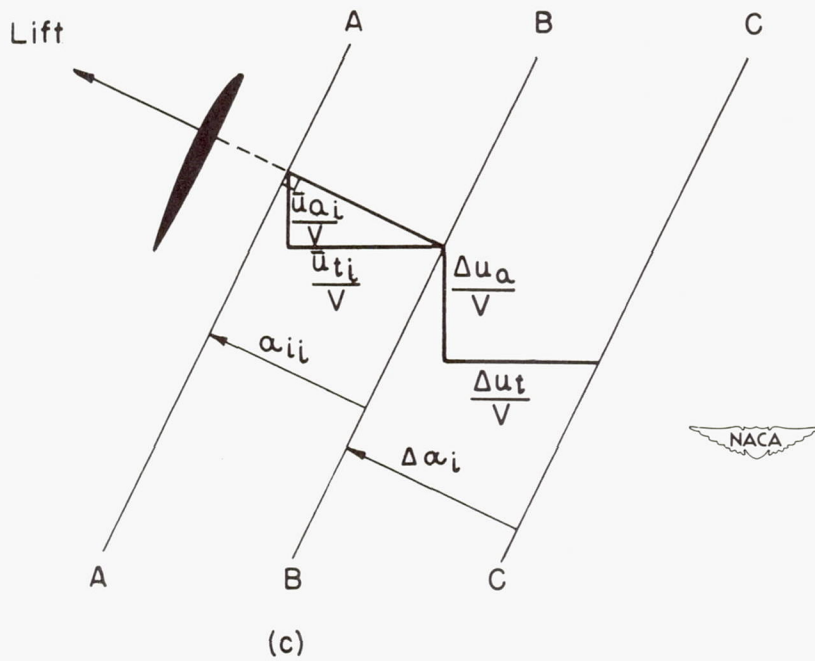
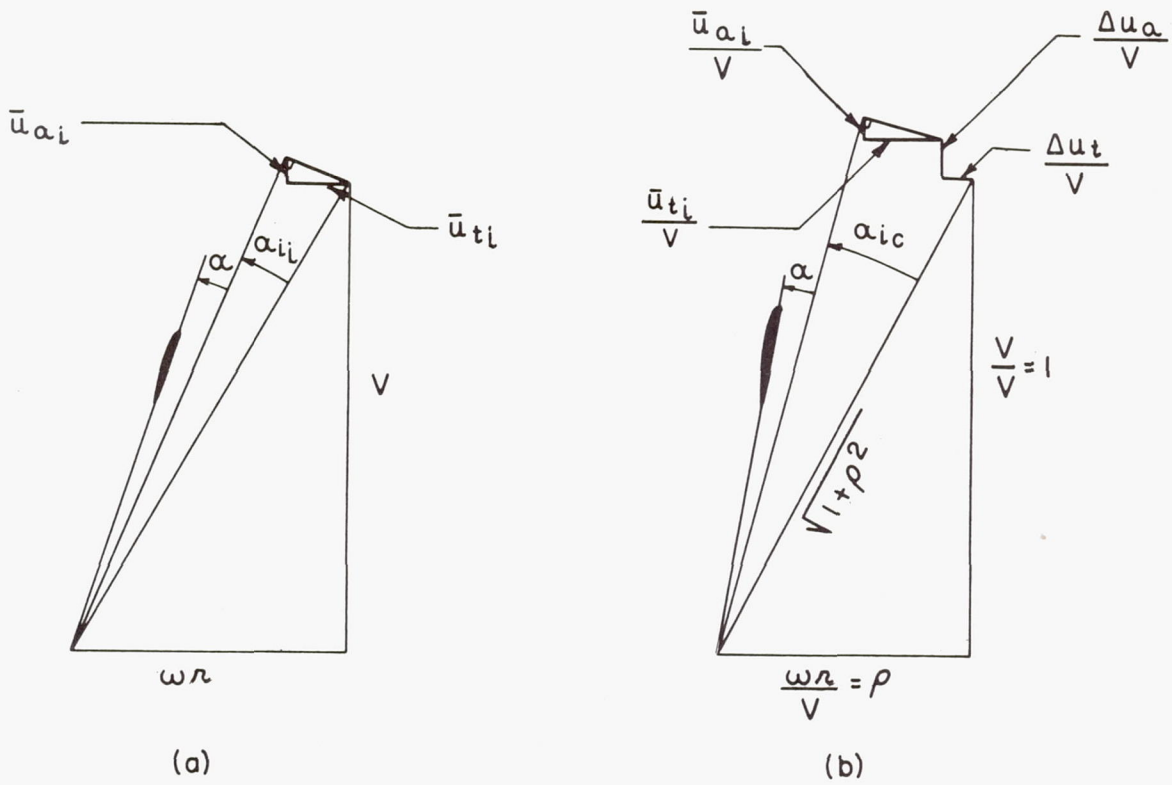


Figure 7.- Induced velocities at the blade.

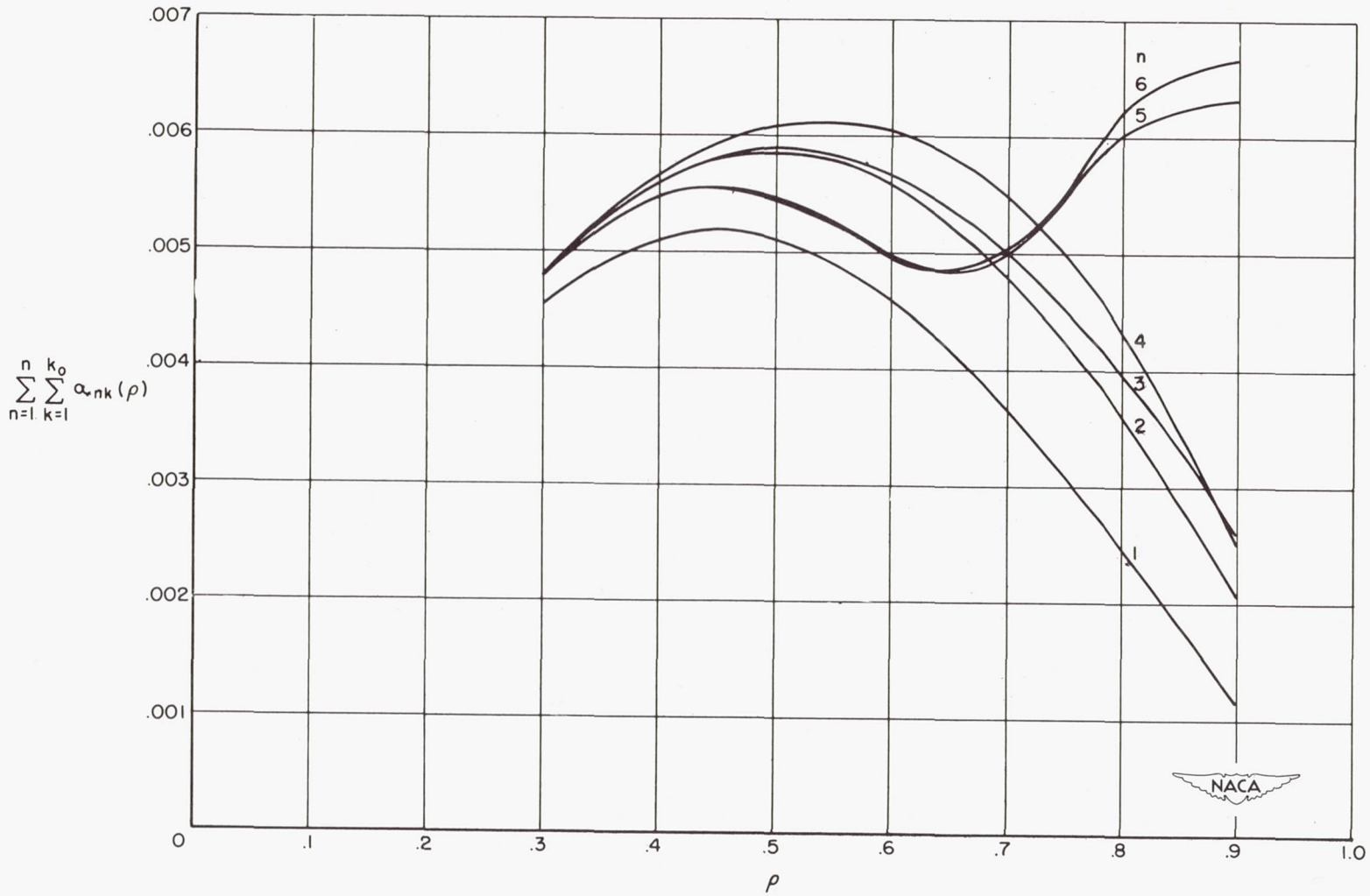


Figure 8.- Partial sums of $\alpha_{nk}(\rho)$, the essential quantity in the induced-angle-of-attack calculation.